Ofioliti An International Journal on Ophiolites and Modern Oceanic Lithosphere

JOURNAL PRE-PROOF

A SNAPSHOT OF THE VOLCANIC ACTIVITY DURING THE EARLY EVOLUTION OF THE LIGURIAN-PIEDMONT OCEAN: INSIGHTS FROM THE PILLOW LAVA SEQUENCE OF THE BALAGNE NAPPE (ALPINE CORSICA)

To appear in OFIOLITI 52, 1 (2027)
DOI: https://doi.org/10.4454/ofioliti.v52i1.592

Received date:	12 December, 2025
Accepted date:	18 April, 2026
First published online	2 September, 2026

A SNAPSHOT OF THE VOLCANIC ACTIVITY DURING THE EARLY EVOLUTION OF THE LIGURIAN-PIEDMONT OCEAN: INSIGHTS FROM THE PILLOW LAVA SEQUENCE OF THE BALAGNE NAPPE (ALPINE CORSICA)

M. Marroni*, L. Pandolfi*,✉, E. Saccani**, E. Sanità *, ***, L. Tagliacollo**

*Dipartimento di Scienze della Terra, Università di Pisa, Italy
** Dipartimento di Fisica e Scienze della Terra, Università di Ferrara, Italy
*** Dipartimento di Scienze, Università G. d'Annunzio Chieti-Pescara, Italy

✉ *Corresponding author, e-mail:* luca.pandolfi@unipi.it

Keywords: *ophiolites, geochemistry, pillow lava basalts, Balagne Nappe, Jurassic, Corsica*

ABSTRACT

In Alpine Corsica, the Upper Units consist of weakly metamorphosed Middle to Late Jurassic ophiolites and their Late Jurassic to Late Cretaceous sedimentary covers. The Navaccia Unit in the Balagne area is one of the best preserved within the Upper Units. It is characterized by a sequence of pillow lava basalts, which is at least 700-800 m thick, which occurs at the top of an oceanic basement, consisting of serpentinized peridotites and gabbros, topped by ophiolitic breccias. This sequence of pillow lavas features dolerite sills as well levels of radiolarites and continental-derived silty sandstones and siltstones.
Geochemically, the Navaccia pillow lavas are mainly tholeiitic basalts with minor basaltic andesites, displaying an overall N-MORB affinity but clear enrichment in incompatible elements such as Ti, Nb, Th, Ta, Hf, and LREE relative to other Corsican ophiolites. Their chondrite-normalized REE patterns, with HREE depletion (Dy_N/Yb_N = 1.29-1.59), indicate a mantle source influenced by residual garnet. Accordingly, based on Dy/Yb vs. Ce/Yb co-variation, the Navaccia basalts can be classified as garnet-influenced basalts like those formed at the ocean-continent transition zone. They are characterized by hump-shaped LREE patterns $(La/Nd)_N$ = 0.64-0.93) indicating source heterogeneity and/or source enrichment. Petrogenetic modelling (Ce, Dy, Yb, Th, and Nb) suggests primary magmas derived from 8-12% partial melting of an enriched spinel-facies mantle, combined with 20-30% melting of a garnet-pyroxenite component. The exceptional thickness and preservation of the sequence enable a chemostratigraphic reconstruction of OCTZ volcanism, revealing uniform incompatible-element contents and Mg# (63-47) throughout the pile. This implies construction through repeated small eruptions tapping magmas with comparable partial-melting degrees and fractional-crystallization histories, likely governed by stable magma-chamber processes. Overall, its geochemistry and the occurrence of continental-derived sediments indicates that the sequence of pillow lavas originated in the initial stage of spreading of the Ligurian-Piedmont oceanic basin, close to the European continental margin.

INTRODUCTION

The Balagne area in northwestern Corsica (Fig. 1) represents one of the key areas in the Alpine-Apennine collisional belt where remnants of oceanic lithosphere, in the form of ophiolitic complexes, are well preserved. It comprises a complex assemblage of tectonic units derived from both the Ligurian-Piedmont oceanic basin and the adjacent European continental margin. Within this framework, the oceanic units represent the uppermost structural level of the Alpine Nappe stack in Corsica. These units are grouped in the Balagne Nappe, which is exposed at the core of a north-south trending synform located southeast of Île-Rousse and west of the Tenda antiform (Rossi et al., 2009). The Balagne Nappe consists of several deformed, weakly metamorphosed units, all of which are characterised by ophiolite sequences and/or their sedimentary cover. In the Balagne Nappe, the ophiolitic units exhibit stratigraphic characteristics that suggest they were situated close the continental margin of Europe plate (Rossi et al., 2002; 2009). This indicates that they were in an ancient ocean-continent transition zone (OCTZ) of the Ligurian-Piedmont oceanic domain (Marroni & Pandolfi, 2007), as has been suggested for other ophiolite sequences within the Alpine-Apennine belt (Manatschal & Müntener, 2009; Amann et al., 2020). Early works have interpreted the pillow lavas from the ophiolite sequences of the Balagne Nappe as transitional-type mid-ocean ridge basalts (T-MORBs) generated during the early stages of oceanic spreading (Venturelli et al., 1979; Durand-Delga et al., 1997). With the term T-MORB these authors intended to highlight the enrichment in light rare earth elements (LREE) relative to medium (M) and heavy (H) REE associated with the early stage of oceanic spreading and the proximity of the continental crust during basalt formation. Later, Saccani et al. (2008) argued that the T-MORB definition does not fully apply to the geochemistry of these basalts because they do not only show LREE enrichment, as most of the TMORB worldwide; rather they also show HREE/MREE depletion. In fact, these authors demonstrated that the geochemistry of these basalts is consistent with the partial melting of a slightly enriched mantle source characterised by garnet-pyroxenite layers (see also Montanini et al., 2008 and Renna et al., 2018 for similar conclusions), or, alternatively, by polybaric partial melting starting in the garnet-facies mantle. Nevertheless, despite geochemical investigations having begun a long time ago (e.g., Venturelli et al., 1979; Durand-Delga et al., 1997; Saccani et al. 2008; Renna et al., 2018), the available geochemical data on the basalts from Balagne Nappe is still limited to few samples.

A spectacular sequence of pillow lava basalts, with minor dolerite sills and scattered thin layers of continental-derived sediments and radiolarites can be seen in the Tartagine and Lagani Valleys (Figs. 2, 3). This sequence represents one of the best-exposed and thickest pillow lava sequence within the Alpine-Apennine ophiolites. However, the geochemistry of these pillow lavas as well as their stratigraphic and structural features remain still unknown.

Understanding the geochemistry, structural architecture, and deformation history of the ophiolites from the Balagne area is crucial for reconstructing the tectonic evolution of the western Mediterranean, particularly about the inception of oceanic spreading processes. Despite decades of geological investigation in this area, the precise mechanisms of emplacement and the internal structural organisation of these ophiolites remain a matter of debate. This study aims to contribute to the ongoing discussion by presenting new, detailed geochemical, structural, and stratigraphic data on the most representative pillow lava sequence of the Balagne Nappe. In this paper, we use field and geochemical data to document the origin of the basalts at the early stages of oceanic spreading. A similar study addressing the temporal variation in chemical composition was proposed by Chalot Prat (2005) for the Chenaillet-Montgenèvre ophiolites in Western Alps. However, though this study presents an excellent chemostratigraphic investigation, it lacks of structural data. Therefore, the study presented here is groundbreaking, as it constitutes the first multidisciplinary investigation to comprehensively examine multiple aspects of one of the thickest and most complete pillow basalt sequences within the OCTZ Alpine Tethys ophiolites. Although this study focuses on the early stages of oceanic spreading, a brief comparison with other ophiolitic basalts from the Ligurian-Piedmont oceanic domain is also provided.

THE OPHIOLITES ALONG THE NORTHERN APENNINES-CORSICA TRANSECT

The ophiolites belonging to the double-verging Alpine belt are well preserved within both Northern Apennines and Corsica (Fig. 1). All these ophiolites are fragments of the Ligurian-Piedmont oceanic basin, which opened between the European and Adria continental margins in the Middle to Late Jurassic period (Stampfli et al. 2002; Bortolotti and Principi, 2005; Dilek and Furnes 2019). The features of these ophiolites suggest that they originated mainly from the interior but also from the edge of the oceanic basin (Marroni and Pandolfi, 2007). All ophiolites from the interior of oceanic basins have the same stratigraphic log, consisting of an oceanic mantle basement intruded by gabbro bodies, covered by a volcanic-sedimentary sequence. The latter consists of ophiolitic breccias that are interfingering with lava flows comprising pillow lava and pillow breccia basalts (Decandia and Elter, 1972; Bortolotti et al., 2001). These ophiolites, which are no more than 1 km thick, are thought to have originated from an ultra-slow spreading ridge during the Middle to Late Jurassic, according to the high volume of serpentinites intruded by pointed km-scale gabbro and sporadic basaltic cover (Treves and Harper, 1994; Tribuzio et al., 2000; Rampone et al. 2020; Rampone and Sanfilippo, 2021). In the Northern Apennines, the ophiolites are well preserved within the Ligurian Units, which overlie the tectonic units detached from the thinned continental margin of Adria plate (Elter et al., 2003). The ophiolites originated from an ultra-slow spreading ridge are preserved in the Internal Ligurian Units where they occur as coherent slices affected by pervasive folding associated with metamorphic imprint ranging from prehnite-pumpellyite to low blueschist facies (Meneghini et al., 2023; Sanità et al., 2024, 2025). The ophiolites also occur as huge slide blocks in the External Ligurian Units, particularly in the Western External Ligurian Units (Marroni et al., 2001). These ophiolites are preserved in Santonian-Campanian sedimentary mélanges, where slide blocks of mantle peridotites, gabbros, and basalts occur alongside slide blocks of granulite and granitoid. According to Marroni et al. (1998) and Marroni and Pandolfi (2007), these sedimentary mélanges originate from a domain consisting of subcontinental mantle peridotites and lower continental crust, which has been intruded by small bodies of gabbro and covered by pillow lava basalts and pelagic sediments. This association between continental and oceanic rocks (Marroni et al., 1998), as well as the geochemistry of the ophiolites (Montanini et al., 2008; Saccani et al., 2015), clearly indicates that they originated from the ocean-continent transition at the thinned continental margin of the Adria plate.

On Corsica Island, the ophiolites only occur on the north-eastern side, i.e., in the Alpine Corsica. They can be found in both the Upper Units and the Schistes Lustrés Complex, albeit in different tectono-metamorphic settings acquired during the alpine orogeny. The Upper Units and the Schistes Lustrés Complex, together with the Lower Units, are thrust onto the European continental margin. This margin is represented by the Hercynian Corsica domain, which consists of a Variscan basement and a volcano-sedimentary cover that has only been marginally affected by Alpine tectonics (Durand-Delga, 1984). In the Upper Units, the ophiolites and their associated sedimentary cover are deformed and metamorphosed at pressure (*P*) and temperature (*T*) pertaining to the prehnite-pumpellyite facies (Marroni and Pandolfi, 2003, Di Rosa et al., 2025). In contrast, the Schistes Lustrés Complex mainly includes oceanic units in which the ophiolites have undergone metamorphism ranging from blueschist to eclogite facies (Caron and Péquignot, 1986; Caron, 1994; Lahondère and Guerrot, 1997). Despite the pervasive deformation and associated metamorphism, the primary features of these ophiolites can still be reconstructed. Most of the ophiolites in the Upper Units (Durand-Delga et al., 2005) and the Schistes Lustrés Complex (Levi et al., 2007; De Cesari et al., 2025), as well as that recently described for the Moglio-Testico Unit in the Southwestern Alps (e.g., Sanità et al., 2022a, 2022b; 2023), exhibit stratigraphic and geochemical characteristics similar to those of the Internal Ligurian Units (Zanzucchi et al., 2025), indicating that they originated from the interior of the oceanic basin. However, Meresse et al. (2012) described some oceanic units of the Schistes Lustrés Complex that show features compatible with their origin from the ocean-continent transition at the edge of the European continental margin. Similarly, the ophiolitic units in the Balagne area, which belong to the Upper Units, have a sedimentary cover whose features indicate that they were located close to the continental margin of Europe (Rossi et al., 2002; 2009; Renna et al., 2017).

GEOLOGICAL SETTING OF THE BALAGNE AREA

In the Balagne area (Fig. 2a, b), the Alpine Corsica is represented by stack of tectonic units that includes the Balagne Nappe and the Palasca Unit, both belonging to the Upper Units (Nardi, 1968; Nardi et al., 1978; Rossi et al., 2001; Marroni and Pandolfi, 2003). This stack, together with the Lower Units, has been thrust onto the Hercynian Corsica (Fig. 2c), which consists of a Variscan continental basement covered by Mesozoic and Early Tertiary sedimentary rocks (Di Rosa et al., 2025).

The pillow lava sequence studied in this paper belongs to the Balagne Nappe, which consists of two weakly metamorphosed oceanic tectonic units, the Toccone and Navaccia Units (Fig. 2c), though Pandolfi et al. (2016) showed that also the Bas-Ostriconi Unit (Fig. 2c) should be included within the Balagne Nappe. To the east, the Balagne Nappe is bounded by a high-angle fault which is interpreted as belonging to the Central Corsica Fault Zone (Fig. 2a). In contrast, to the west, the Balagne Nappe is thrust onto the Hercynian Corsica, together with the Palasca Unit and the Lower Units.

The stratigraphy of the oceanic units has been reconstructed by assembling all the stratigraphic logs from the different units and subunits of the Balagne Nappe (Nardi et al., 1978; Durand-Delga, 1984; Rossi et al., 2001; Marroni and Pandolfi, 2003). This sequence (Fig. 2c) includes the ophiolite and its sedimentary cover. The ophiolite sequence consists of a basement of strongly serpentinized peridotites, alongside small bodies of gabbro. This basement is covered by a thin layer of ophiolitic sedimentary breccia and a thick succession of pillow lava basalts. This sequence is Middle to Late Jurassic in age (Rossi et al., 2009) and it is covered by Chert, Calpionella Limestone and San Martino Formations ranging in age from Late Jurassic to Early Cretaceous (Durand-Delga, 1984; De Wever et al., 1987; Marroni et al., 2000; Peybernès et al., 2001). These hemipelagic deposits are characterized by intercalation of fine- to coarse-grained sedimentary breccias which are thought to have been supplied by the European continental margin, as suggested by the U-Pb geochronology of detrital zircons in arenites (Renna et al., 2017). This feature sets the ophiolites of the Balagne Nappe apart from those of the other Upper Units. The San Martino Formation grades upward to Lydienne Flysch, Toccone Breccia, and Novella Sandstone Formations. represented by siliciclastic and carbonite turbidites ranging in age from Early to Late Cretaceous (Durand-Delga, 1984; Marino et al., 1995). According to Pandolfi et al. (2016), the Campanian Narbinco Flysch Formation, including the Cima Lo Caigo Conglomerate Fm., of the Bas-Ostriconi Unit is the youngest deposit in the ophiolite sedimentary cover.

The deformation history of the Balagne Nappe was first described by Waters (1990) and Egal (1992), and subsequently reconstructed in detail by Marroni and Pandolfi (2003), as well as by Pandolfi et al. (2016). This deformation history was identified in all units of the Balagne Nappe, including the Bas-Ostriconi Unit, with no significant differences observed. These authors have identified a polyphase deformation history comprising several phases, referred to as D1, D2 and D3. The D1 phase is characterized by non-cylindrical, tight to isoclinal folds with subrounded and thickened hinge zones. The F1 folds are characterized by well-developed, continuous S1 axial-plane foliation that, in shales, can be classified as slaty cleavage. In the basalts, widespread static recrystallisation occurred during the D1 phase involving prehnite, pumpellyite, quartz, albite, calcite, and Fe-oxides (Dal Piaz et al., 1977). The D1 mesoscopic structures generally face west to north-west. The D1 phase structures underwent deformation during the D2 phase, which is the most widespread in the field. This phase is characterized by asymmetric and overturned F2 folds with rounded to acute hinges and steep axial planes. The A2 fold axes mainly trend N-to-S and are associated with S2 axial-plane foliation, which, in shales, can be recognized as crenulation cleavage. In more competent lithologies, such as basalts, the S2 foliation is represented by a disjunctive cleavage. The D2 folds face west. The D3 phase (referred to as the D4 phase in Marroni and Pandolfi, 2003) is represented by asymmetric F3 folds which typically exhibit clear eastward vergence. Their axial planes occur as sub-horizontal or gently dipping planes everywhere. The A3 fold axes tend to range from NNE/SSW to NNW/SSE.

Di Rosa et al. (2025) recently estimated the metamorphic peak acquired during the D1 phase in the Balagne Nappe by analyzing the composition of selected chlorite-white mica pairs using Vidal and Parra (2000) multi-equilibrium method. In these units, the *P-T* conditions were estimated 0.55-0.60 GPa and 240-260 °C for the Navaccia Unit, 0.50-0.60 GPa and 250-270 °C for the Toccone Unit and 0.35-0.50 GPa and 215-250 °C for the Bas-Ostriconi Unit, which are coherent with prehnite-pumpellyite metamorphic facies conditions.

METHODS

We have applied a multidisciplinary approach by combining fieldwork and whole rock geochemical analyses. Fieldwork has been carried out along the Lagani and Tartagine Valleys covering about 20 km^2.The geological survey has been performed using a 1:10.000 topographic map and by applying the classic field techniques to build a detailed geological and structural map of the study area. Samples of basalt and dolerite, as well as the associated sedimentary rocks, have been collected in the study area for microscopic analysis.

Whole-rock major elements and selected trace elements were analyzed by X-ray fluorescence (XRF) on pressed-powder pellets using an ARL Advant-XP+ automated X-ray spectrometer. Major elements were determined on fused glass discs prepared with a mixture of 66% dilithium tetraborate ($Li_2B_4O_7$) and 34% lithium metaborate ($LiBO_2$), using a sample-to-borate dilution ratio of 1:11. Fusion was performed in a Pt_{95}-Au_5 crucible with an Equilab F1-Fluxer automatic apparatus. The matrix correction method proposed by Lachance and Trail (1966) was applied. Trace elements were analyzed on pressed-powder pellets, while volatile contents were determined as loss on ignition (L.O.I.) at 1000°C.

Rare earth elements (REE) and selected trace elements (Rb, Sr, Zr, Y, Nb, Hf, Ta, Th, U) were analyzed by inductively coupled plasma-mass spectrometry (ICP-MS) using a Thermo iCAP-TQ spectrometer. All whole-rock analyses were conducted at the Department of Physics and Earth Sciences, University of Ferrara, and the results are presented in Table 1. The accuracy of the XRF and ICP-MS data was evaluated by analyzing international standard rocks as unknowns. Detection limits for XRF and ICP-MS analyses were determined from multiple runs of twenty-nine international standards. Accuracy and detection limits are provided in Supplementary Table S1. For the discussion of the geochemical characteristics of the studied rocks, major element compositions were recalculated on an L.O.I.-free basis.

RESULTS

The ophiolite crustal section

The crustal section of the ophiolites of Navaccia Unit has been reconstructed in the Tartagine Valley outcrops for the lower sequence and in the Lagani Valley outcrops for the middle and upper sequences (Figs. 3, 4). All the studied outcrops belong to the Navaccia Unit. This section (Fig. 4) is mainly composed of pillow lava basalts (hereafter referred as Navaccia pillow lavas), with minor dolerite sills and scattered thin layers of continental-derived sediments and radiolarites.

At the Carnispola bridge in the Tartagine Valley, the transition from intrusive rocks to pillow lava basalts is clearly visible along the roadcut (Rossi et al., 2009). The intrusive rocks are represented by medium- to coarse-grained Mg-gabbros, which exhibit rough layering enhanced by variations in grain size and/or mineral composition. The gabbros are covered by fine-grained sedimentary breccia (Fig. 4) that is less than 5 m-thick and consists of angular fragments of Mg-gabbros, Fe-gabbros and trondhjemites. Rossi et al. (2002) determined an age of 169 ± 3 Ma for the zircons in the trondhjemite using the U/Pb method.

A thick sequence of pillow lava basalts, exposed along the Lagani Valley section, sharply tops the sedimentary breccia. The thickness of the entire sequence of pillow lava basalts cannot be accurately estimated due to the occurrence of several high-angle faults. Nonetheless, a thickness of at least 700-800m can reasonably be assumed (Fig. 4). This sequence begins with a 10-metre-thick layer of massive basalts. This layer is topped by pillow lava basalts, which consist of closely packed, irregularly shaped, bent and squeezed pillows, each measuring less than 1 m in diameter (Fig. 5a). The pillows are characterized by a convex and rounded upper surface and a tapered base, which clearly indicate the paleo-horizontal attitude. The pillows display a more crystalline core, which is bounded by a dark green rim. Lineations or scrape marks form on their sides during extrusion. Some of the pillows exhibit intra-pillow cavities containing fine-grained volcaniclastic material. The spaces between the pillows consist of hyaloclastite bands made up of glass shards and basaltic fragments in a fine-grained matrix. Most of the pillows are characterized by a dense network of fractures on their rims. According to this occurrence, levels less than 2-3m thick of pillow breccia can be found (Fig. 5b). This breccia is clast-supported and consists of a monomict assemblage of pillow fragments. The clasts range in size from a few centimetres to a few decimetres.

The dolerite sills, up to 40-50 m thick, occur as two bodies (Figs. 3, 4) with lenticular shape, both characterized by medium-grained, holocrystalline texture without evidence of layering or grain-size variations (Fig. 5c). The long base of these bodies is roughly parallel to the paleo-horizontal attitude detected in pillow lava basalts. A swarm of dikes, each a few centimetres thick, has been found cutting through the dolerite (Fig. 5d). The presence of fragments of the host rock and chilled margins characterizes these aphyric dikes.

An intercalation of greenish siltstone and silty sandstone occurs in the uppermost portion of the pillow lava sequence (Figs. 4, 5e). This sedimentary body displays limited lateral continuity, with a thickness varying from 0 to 1.5 m (Fig. 5e). The intercalation is structureless, showing no primary sedimentary features; however, bioturbation is clearly present. In thin section, the silty sandstones correspond to arkosic composition, consisting of quartz, feldspars (undifferentiated), and white mica clasts embedded in a recrystallized matrix dominated by brownish clay minerals (Fig. 5f); ophiolite-derived fragments are not present. Within the silt layers, fragments of organic matter are locally preserved. Bioturbation is further emphasized by the widespread occurrence of organic-rich patches, which likely represent remnants of burrowing activity (Fig. 5g white arrow). In addition, an intercalation of red bedded cherts (Figs. 4, 5h), less 1m thick, has also been found at the uppermost level of the pillow lava sequence.

At the top of the pillow lava sequence, there is a level of pillow breccia that is overlain by a sedimentary sequence comprising Chert, Calpionella Limestone and San Martino Formation. This sequence is clearly visible along the railway cut at the km 59 of the Routes Territoriales RT301(ex Routes Nationales RN197) (Peybernès et al., 2001). The pillow breccia exhibits stratigraphic relationships with the Chert Formation through the presence of a thin level where fragments of pillow that are interspersed within a siliceous mudstone. The Chert, about 20m thick, ranges in age from the Middle-Upper Callovian to the Tithonian (De Wever et al., 1987). The Chert Formation grades up to Calpionella Limestone, San Martino Formation, and Lydienne Flysch, ranging in age from Tithonian to Barremian. These formations consist of carbonate and siliciclastic turbidites characterized by intercalations of coarse-grained breccias where continental-derived fragments of rhyolites, granitoids, micaschists, and amphibolites have been found (Peybernés et al., 2001). The first order feature of this sedimentary cover is its abundant continental debris, which originated from the European plate.

The whole sequence of pillow lava basalts is folded and cut by several strike-slip faults (Fig. 3). The folds, as shown by the attitude of the pillow lavas (Fig 6), are characterized by short steep (Fig 6b,c), sometime overturned, limbs with wide normal limbs characterized by a dip up to 30° (Fig 6a, c). These folds are characterized by an axis showing a NE-SW direction and gently plunging toward NE, whereas the attitude of the axial planes is toward E-SE sectors (Fig. 6c). According to their westward vergence, these folds can be regarded as developed during the D2 phase described by Marroni and Pandolfi (2003). The strike-slip faults exhibit an N-S trend and are likely to be related to the fault system of the Central Corsica Fault Zone (Figs. 2a,3).

Petrography

The Navaccia pillow basalt sequence primarily consists of pillow lavas with a minor presence of doleritic sills. All samples exhibit extensive alteration due to low-grade ocean-floor metamorphism and hydrothermal processes, leading to significant modification of the original mineral assemblages. However, the primary igneous textures remain well preserved. For clarity, the prefix "meta-" will be omitted when referring to these rocks.

Mineralogical alterations have largely replaced plagioclase with albite and calcite, or alternatively with sericite, prehnite, and clay minerals. Olivine and clinopyroxene are typically altered to chlorite, though in some cases, clinopyroxene has transformed into tremolite amphibole. Nonetheless, a few samples retain relics of seemingly fresh clinopyroxene. The hyalophitic groundmass is often replaced by an assemblage of chlorite and clay minerals.

In terms of texture, the pillow basalts range from aphyric to moderately porphyritic (phenocryst index, PI <10%) and porphyritic (PI up to 40%). The porphyritic varieties are marked by plagioclase phenocrysts present in all samples (Fig. 7a), with some also containing olivine and clinopyroxene phenocrysts. Sample CO151 features plagioclase phenocrysts displaying both euhedral and skeletal forms. Olivine phenocrysts tend to be relatively small, while plagioclase and clinopyroxene phenocrysts exhibit a broad grain-size spectrum, from microphenocrysts (~50 µm) to approximately 2 mm (Fig. 7a). The groundmass in both aphyric and porphyritic basalts varies in texture. Some samples exhibit a hyalophitic groundmass, characterized by small radiating plagioclase laths within a glassy matrix (Fig. 7b). Commonly, the samples display a microcrystalline ophitic groundmass (Fig. 7c). Additionally, variations such as ophitic to sub-ophitic, sub-ophitic to intergranular, and purely intergranular (Fig. 7d) textures are observed. The groundmass crystal size varies from very fine-grained to medium-grained across different samples.

Doleritic sills exhibit a granular doleritic texture, characterized by coarse-grained crystals (1-4 mm) and poikilitic clinopyroxene (Figs. 7e, f). Small calcite veins and dispersed amygdules filled with calcite (rarely) or zeolite (more frequently) are common in all samples. The crystallization order in all samples is: olivine ± plagioclase + clinopyroxene, which is the characteristic crystallization order of rocks formed at mid-ocean ridge settings (Beccaluva et al., 1983).

Geochemistry

A reliable method for investigating the geochemistry and petrology of these rocks is to use the immobile elements. They include high field strength elements (HFSE; such as, Ti, P, Zr, Y, Sc, Nb, Ta, Hf, Th), certain transition metals (e.g., Ni, Co, Cr, V), and the REE (e.g., Pearce and Norry, 1979; Shervais, 1982).

The Navaccia pillow lava sequence is primarily composed of basalts, with minor basaltic andesites, exhibiting SiO_2 concentrations ranging from 48.12 to 54.87 wt%. These rocks display a predominantly sub-alkaline, tholeiitic character, as indicated by their low Nb/Y ratios (0.11-0.21; Fig. 8) and high Ti/V ratios (38-70, Table 1), which are consistent with tholeiitic basalts from mid-ocean ridge settings (Shervais, 1982). MgO contents vary between 3.56 and 7.15 wt%, while Mg# [Mg# = 100 * molar ratio of MgO / (MgO + FeO)] falls within a relatively narrow range of 63 to 52 for most samples (Table 1). Sample CO154 exhibit a notably low Mg# value of 39 (Table 1). However, this sample represent the outermost rim of a pillow and therefore, its Mg# is most likely influenced by secondary alteration. These Mg# values suggest that most of these rocks represent magmas formed within a constrained range of magmatic fractionation, which can be roughly estimated as ranging from 12 to 25% (see Groove and Bryan, 1983; Langmuir et al., 1992; Zhang et al., 2009).

All samples exhibit an increase in incompatible elements (e.g., TiO_2, P_2O_5, Y, Nb, V) with increasing Zr, which is used here as a differentiation index. In contrast, Ni and Cr show a marked decline with increasing Zr. FeO_t contents increase from the less evolved basalts (Mg# > 60) to the moderately evolved basalts (Mg# < 60). The tholeiitic fractionation trend is generally characterized by a gradual rise in iron content in moderately fractionated rocks, followed by a sharp decline in more evolved basaltic andesites and ferrobasalts. However, the Navaccia basaltic rocks do not display a decrease in FeO_t = [FeO + Fe_2O_3] content with increasing fractionation, further suggesting that these rocks represent melts that underwent moderate degrees of differentiation. Moreover, the limited variation in Al_2O_3/TiO_2 (7-13) and Ti/1000 (8-14) indicates a fractionation trend primarily controlled by the progressive crystallization of plagioclase and clinopyroxene, with minimal involvement of magnetite (Beccaluva et al., 1983; Barbero et al., 2020). Overall, the Navaccia basalts exhibit moderate chemical variability, as reflected by their TiO_2 (1.36-2.26 wt%), P_2O_5 (0.16-0.31 wt%), Zr (81.6-147 ppm), and Y (21.5-36.5 ppm) contents.

In the N-MORB normalized (Sun and McDonough, 1989) incompatible element spider diagrams (Figs. 9a-d), the Navaccia basaltic rocks display a relatively flat pattern from Th to Ti (e.g., Th_N/Ti_N = 1.04-2.36). HFSE contents are low, ranging from ~1 to ~4 times the N-MORB composition (Sun and McDonough, 1989). However, heavy REE (Tb and Yb) and Y contents are notably low, ranging from ~1 to ~0.5 times the N-MORB composition, and show sharply decreasing trends from Tb to Yb (Figs. 9a-d). Chondrite-normalized REE patterns (Sun and McDonough, 1989; Figs. 9e-h) are characterized by HREE depletion relative to LREE and MREE, with $(Sm/Yb)_N$ and $(La/Yb)_N$ ratios ranging from 1.63-2.37 and 1.11-2.29, respectively. The LREE exhibit convex-upward trends (Figs. 9e-h), as evidenced by $(La/Nd)_N$ ratios between 0.64 and 0.93. The Chondrite-normalized REE patterns of the Navaccia basalts significantly differ from those of both N-MORB and E-MORB (see Fig. 9e). These geochemical characteristics are further summarized in the binary plots of $(La/Nd)_N$ vs. $(La/Yb)_N$ and $(Nd/Yb)_N$ vs. $(La/Yb)_N$ in Fig. 10.

All samples exhibit a negative Eu anomaly (Figs. 9e-h), indicative of early plagioclase crystallization and removal. In the discrimination diagram (Fig. 11), these basalts plot within the field for subduction-unrelated basalts, positioned between the compositions of typical N-MORB and E-MORB (Sun and McDonough, 1989). Nonetheless, the pronounced fractionation of HREE relative to MREE suggests a significant garnet signature, implying the melting of a heterogeneous mantle source containing garnet-bearing mafic and ultramafic layers (Montanini et al., 2008; Saccani et al., 2008). Consistently, in the discrimination diagram in Fig. 12, the Navaccia basalts are classified as garnet-influenced basalts like those formed at the ocean-continent transition zone (Saccani, 2015).

DISCUSSION

Geochemical comparison with basaltic and metabasaltic rocks from Alpine Corsica and Northern Apennine Ligurian units

A comparison of the geochemical features of the Navaccia pillow lavas with equivalent rocks from other ophiolitic and metaophiolitic units in both Corsica and the Northern Apennines provides insight into similarities and differences among these units. Such comparisons can, in turn, help reconstruct their petrogenetic processes and their possible original paleogeographic setting within the Alpine Tethys. Notably, the basaltic rocks of the Navaccia pillow sequence show no chemical differences from pillow basalts in other areas of the Balagne Nappe, such as Col di San Colombano and Punta di Pietralba (Saccani et al., 2008), Piana di Castifao (Durand-Delga et al., 1997), and elsewhere (Renna et al., 2018) (see Figs. 8, 10-14). Consequently, the basalts from these localities of the Balagne Nappe are treated here together with the rocks investigated in this study and referred as Balagne basalts.

At first glance, the Balagne basalts appear more enriched than basalts from other ophiolitic and metaophiolitic units of Corsica and Northern Apennine, except for some basalts from the Nebbio Unit in Corsica (Saccani et al., 2008) and from the External Ligurian Units in the Northern Apennines (Montanini et al., 2008). They are characterized by relatively higher Ti/Y and Nb/Y ratios, plotting toward E-MORB compositions and the OIB field in Fig. 8). Selected incompatible elements plotted against Zr (used here as a differentiation index; Fig. 13) show that the Balagne basalts are enriched in Ti, Nb, Th, Ta, Hf, and Ce (LREE) relative to basaltic and metabasaltic rocks from other Alpine Corsica ophiolitic and metaophiolitic units and the Internal Ligurian units of Northern Apennine. While the Nebbio Unit basalts have Ti, Nb, and Th contents comparable to those of the Balagne basalts, they display significantly higher Zr contents (Figs. 13a-c). By contrast, the Nebbio Unit basalts are more enriched in Ta, Hf, and Ce than the Balagne basalts (Figs. 13d-f). These enrichments do not appear to be related to the degree of fractionation, as the Nebbio basalts are generally less fractionated than those studied in this paper.

When compared with External Ligurian basalts, the Balagne basalts show strong similarities in several elements: particularly, Ta, Hf, and Ce (Figs. 13d-f), as well as broad similarities in Nb and Th (Figs. 11, 13b-c). The co-variation of Th, Ta, Nb, Hf, La, and Ce with Zr demonstrates that the Balagne basalts are enriched in these elements (and in incompatible elements and LREE more generally) relative to other Alpine Corsica ophiolitic and metaophiolitic rocks and Internal Ligurian basalts, as well as to the N-MORB composition of Sun and McDonough (1989) (Fig. 13). Interestingly, the Balagne basalts do not plot between N-MORB and E-MORB compositions. Instead, they fall along the N-MORB-OIB array, closer to N-MORB (Figs. 13b-f).

The Balagne basalts are further characterized by Th/Ta ratios like those of basaltic rocks from other Alpine Corsica ophiolitic and metaophiolitic units and Internal Ligurian basalts, indicating that no selective enrichment of Th over Ta occurred (Fig. 14). In contrast, relative to both Alpine Corsica and External Ligurian metaophiolitic and ophiolitic units, the Balagne basalts show marked enrichment in Th (and Ta, not shown) with respect to MREE (Th/Tb in Fig. 14).

Chemostratigraphy

The Navaccia Unit of the Balagne Nappe shows one of the best-exposed, best-preserved, and thickest pillow lava successions within the ophiolites derived from the Ligurian-Piedmont basin. As such, it provides a natural laboratory for applying a chemostratigraphic approach. The reliability of this approach has important implications for understanding the ocean-floor volcanism at the OCTZ of the Ligurian-Piedmont basin, as it reveals the degree of compositional homogeneity in magmas erupted during different volcanic events. This, in turn, allows us to better constrain temporal variations in composition, geochemical signatures, and partial melting conditions of the mantle source.

Although individual volcanic events cannot be distinguished in the field, the Navaccia pillow lava sequence is interpreted as the product of multiple small eruptions, by analogy with modern slow and ultra-slow spreading ridges (e.g., Atlantic Ocean, Flower et al., 1980).

Because the studied rocks correspond to magmas at different stages of fractionation, absolute elemental concentrations cannot be directly used for this purpose, as they are influenced by the extent of fractionation of olivine and plagioclase. To address this, the effects of low-pressure crystal fractionation on incompatible element concentrations must be removed. This is done by recalculating the concentrations to 8 wt% MgO along the fractionation vector, following an approach like the Fe_8 and Na_8 parameters of Klein and Langmuir (1987). For this chemostratigraphic study, we selected TiO_2, Nb, Th, and Ta. Conversely, ratios of highly incompatible, immobile elements are only weakly affected by moderate degrees of magmatic fractionation, partial mantle melting, or alteration processes, and are generally considered to reflect source characteristics (Allègre and Minster, 1978; Joron and Teuil, 1989). For this reason, we used Nb/Tb, Th/Tb, and Ta/Tb ratios (Fig. 15). In addition, to assess the role of residual garnet in the mantle source, we employed TiO_2/Yb and chondrite-normalized $(Dy/Yb)_N$ ratios, as proposed by Pearce (2008) and Saccani (2015), respectively.

No systematic stratigraphic variation is observed in the abundances of the selected incompatible elements or in their ratios (Fig. 15). The Mg# values also display very limited variability: 21 out of 23 samples fall within the mean ± standard deviation, while sample CO146 shows slightly lower value. Sample CO154 displays a significantly lower value, reflecting strong alteration at the pillow rim (Fig. 15). Therefore, its chemical features cannot be regarded as significant. This suggests that each eruptive unit within the Navaccia pillow lava sequence produced basaltic rocks characterized by a similar degree of fractionation (12-25% for most of the samples). This seems to be a common feature for basalts from different tectonic units of the Balagne Nappe (see Durand-Delga et al., 1997; Saccani et al., 2008). Indeed, the occurrence of only one fractionated ferrobasalt has so far been reported in literature (Renna et al., 2018). Ti_8, Nb_8, Th_8, and Ta_8 display only minor variations throughout the stratigraphic sequence, with all four elements following similar trends (Fig. 15). These elements show a general enrichment relative to the N-MORB composition of Sun and McDonough (1989) (Fig. 15). However, when comparison is made, all the sampled basalts exhibit Ti_8 contents significantly higher than that of the N-MORB, whereas the Nb_8, Th_8, and Ta_8 contents are comparable to those of N-MORB in a few samples (e.g., CO159, CO158C, CO149, CO152). Likewise, ratios of Th, Ta, and Nb with Tb (MREE) show little variation from bottom to top (Fig. 15) and follow similar trends. These ratios are always higher than those of the typical N-MORB (Sun and McDonough, 1989).

The TiO_2/Yb and chondrite-normalized Dy/Yb ratios show very minimal stratigraphic variation and both ratios are significantly higher than those of the N-MORB (Sun and McDonough, 1989). Moreover, the Ti/Yb ratios exceed the discriminant boundary between low Ti/Yb MORB and high Ti/Yb OIB of Pearce (2008). According to Pearce (2008) these high Ti/Yb ratios indicate that the Navaccia basalts may have originated by melting beneath thicker or hotter lithosphere and with residual garnet. Likewise, the Dy/Yb ratios are higher than the discriminant boundary between N-MORB formed at mid-ocean ridge and G-MORB erupted at the OCTZ in the Ligurian-Piedmont (Saccani, 2015).

In summary, the chemostratigraphic study shows no evidence of discontinuity in the chemical stratigraphy the Navaccia pillow lava sequence. This sequence was likely formed through a series of small eruptions, each producing flows of relatively uniform composition, reflecting comparatively uniform conditions of partial melting and source composition. The relative uniformity of the Mg# throughout the stratigraphy suggests stable cycling between magma recharge and differentiation within the magma chamber prior to eruptions.

Petrogenesis

A primary distinguishing feature of the Navaccia basalts is their pronounced depletion in HREE relative to MREE (e.g., DyN/YbN = 1.29-1.59). This pattern can be attributed to varying degrees of influence from a garnet-bearing signature in their mantle sources (e.g., Montanini et al., 2008). According to Saccani et al (2008), the garnet signature observed in similar G-MORBs from various units of the Corsica ophiolites and metaophiolites is mainly the result of partial melting of a depleted MORB mantle source heterogeneously composed of garnet-bearing mafic to ultramafic layers. However, the authors did not rule out the possibility that minor volumes of the Corsica basalts may have originated through polybaric melting, beginning within the garnet peridotite stability field, and continuing into the spinel peridotite facies.

Partial melting models can help to constrain the possible composition of the mantle source and the melting processes responsible for the formation of the Navaccia pillow lava sequence. However, a precise quantification of these processes remains challenging due to the difficulty in accurately characterizing compositions and melting conditions of the mantle source. A main limitation is in the definition of the composition of garnet-bearing mafic to ultramafic layers potentially involved in the melting processes, as they typically display significant compositional variability (e.g., Liu et al., 2005).

Other distinguishing features of the Navaccia pillow lavas are their pronounced hump-shaped LREE patterns (Figs. 9e-h) and their enrichment in Ti, Nb, Th, Ta, Hf, La, and Ce compared to basalts and metabasalts from Northern Apennine and Corsica (Fig. 13). A hump-shaped pattern in the LREEs suggests source heterogeneity, often linked to the presence of enriched domains or metasomatic components. Enriched domains may include pyroxenite veins, recycled oceanic crust, or hydrous metasomatic phases that contribute selectively to the LREE budget (e.g., Zindler and Hart, 1986; Stracke et al., 2005). Studies have shown that both spinel- and garnet-pyroxenites and other recycled lithologies within the upper mantle can impart distinctive LREE patterns during mantle partial melting, depending on their modal mineralogy and the degree of melting (e.g., Liu et al., 2005). Spinel pyroxenites representing clinopyroxene-rich cumulates likely derived from LREE-enriched basaltic magmas show LREE-enriched and convex patterns (Xu, 2002; Liu et al., 2005; Fig. 16a). Another possible explanation for hump shaped LREE patterns is interaction with crustal materials during magma ascent or storage. If a mantle-derived melt assimilates felsic crustal components (e.g., granitoids, sedimentary rocks), this can selectively enrich the melt in certain LREEs, resulting in non-linear patterns with local humps in La-Sm or Ce-Nd. The specific shape depends on the nature and amount of assimilated material and the degree of fractional crystallization (e.g., Rudnick and Fountain, 1995). Distinguishing source enrichment from crustal contamination in basalts is challenging, as both processes can produce similar geochemical signatures. Radiogenic isotopes are the most powerful tool to differentiate between mantle source characteristics and crustal assimilation (see Renna et al., 2018). However, a study of the isotopic composition of the Navaccia pillow lavas is beyond the scope of this paper and will be developed in detail in future research. In the absence of the isotopic composition, a multi-parameter approach combining trace elements and geological context can be applied to discriminate these different processes.

Certain trace element and trace element ratios are sensitive to crustal input or mantle source characteristics. Enrichment in Ti, Nb, Th, and Ta is indicative of source enrichment by metasomatic components. High Th/Nb (>0.2) or La/Nb (>1.5) values are typical of crustal contamination, whereas mantle enrichment produces lower ratios (Hofmann et al., 1988). Our samples show low Th/Nb (<0.08) and La/Nb (<1.39) values, which suggest mantle source enrichment. Accordingly, the enrichment in some key elements, such as Ti, Nb, Ta, and Th relative to Zr (Fig. 13) further points out for mantle source enrichment (e.g., Pearce, 2008). This conclusion is also supported by Renna et al. (2018) who, based on Nd isotopes, argued against processes of crustal contamination affecting Balagne doleritic sills. Nonetheless, the OCTZ geodynamic setting in which the studied pillow sequence formed, generally favours crustal contamination. Therefore, though the geochemical evidence argues against crustal contamination, in the lack of radiogenic isotope data for the studied sequence, this process cannot be unequivocally ruled out for the Navaccia Unit.

Despite the limitations discussed above, semi-quantitative modelling based on selected incompatible elements and REEs can still provide a first-order approximation of the mantle source composition (in terms of enrichment or depletion and the possible occurrence of residual garnet), as well as insights into melting processes. Because of their higher LREE/HREE ratios relative to N-MORB, similar rocks from the Corsica and Northern Apennine ophiolites have been interpreted by several authors as transitional or enriched MORBs, produced from slightly enriched mantle sources during the initial stages of oceanic spreading (e.g., Beccaluva et al., 1977; Venturelli et al., 1979, 1981). Based on the incompatible element characteristics of the studied basalts (Figs. 13, 14) and on the general petrogenetic framework previously proposed for the Corsica and Northern Apennine ophiolites (Montanini et al., 2008; Saccani et al., 2008), we suggest that a MORB-type mantle source enriched in LREE, Th, Ta, and Nb represents the most plausible source.

In our modelling, we used a theoretical mantle source composition corresponding to a depleted MORB mantle (DMM, Workman and Hart, 2005), but with LREE, Th, Ta, and Nb contents corresponding to those of the Primordial Mantle (PM) of Sun and McDonough (1989) (Fig. 16a). For this modelling, we adopted garnet-pyroxenite compositions from Liu et al. (2005), selected as the best match for reproducing the overall geochemical characteristics of the most primitive basalts from the Navaccia pillow lavas (Fig. 16a). Three basalts were chosen to this purpose (CO159, CO159A, CO162). However, these basalts do not represent truly primitive melts. Therefore, the composition of their primitive parental melts was calculated assuming 12-16% fractional crystallization of olivine + plagioclase + clinopyroxene. In our modelling, we also considered as possible alternative mantle sources a pure DMM (Workman and Hart, 2005), and a PM (Sun and McDonough, 1989). Source compositions, melting condition, and partition coefficients are provided in the caption of Fig. 16.

Modelling the whole REE spectrum is not feasible, as the nature of the hump-shaped pattern in the LREEs cannot be constrained with the available data. Nevertheless, the LREE/HREE vs. MREE/HREE ratios (Fig. 16b) and Th content vs. Nb/Yb ratio (Fig. 16c) are particularly useful for modelling the garnet signature in melting processes and assessing the degree of mantle source enrichment. Th and Nb abundances and the Ce/Yb ratio are used as indicators of the source enrichment, whereas Dy/Yb and Nb/Yb ratios are sensitive to the presence of residual garnet in the source.

Non-modal batch partial melting model using Ce/Yb and Dy/Yb ratios (Fig. 16b) indicate that the compositions of the primitive basalts are consistent with 8-15% partial melting of the theoretical mantle source in the spinel-facies, combined with melts derived from 20-30% degree of melting of a garnet-pyroxenite component. Results from the Th-Nb-Yb modelling (Fig. 16c) agree with those obtained from REE modelling (Fig. 16b). The Th and Nb contents of the primary melts are indeed consistent with mixtures of melts derived from 8-12% non-modal batch partial melting of the enriched theoretical mantle source in the spinel-facies and melts resulting from 20-30% melting of a garnet-pyroxenite component. In both REE and T-Nb modellings we estimate that the contyribution of the garnet-pyroxenite derived melt to the bulk melt composition was in the range 5-10%.

REE and Th-Nb modelling (Figs. 13b, c) indicate that the alternative mantle source compositions or different melting conditions cannot account for the observed chemical features of the Navaccia Unit basalts. For instance, melting of a pure DMM source in the spinel facies or a DMM source undergoing initial melting in the garnet-facies followed by higher-degrees melting in the spinel-facies (under various combinations of melting fractions), or even a DMM source containing garnet-pyroxenite layers, could only reproduce the chemistry of the Balagne primary melts by invoking unrealistically low degrees (<2.5%) of the DMM partial melting.

Conversely, a PM source could reproduce the REE compositions of the Balagne basalts only if very high degrees of melting (>20%) occurred in the garnet-facies, followed by an additional 20% partial melting in the spinel-facies (Fig. 16b). Similarly, the Th-Nb covariation observed in the Navaccia Unit basalts cannot be explained by partial melting of a PM source (Fig. 16c). However, the REE compositions of the Navaccia Unit basalts could alternatively be accounted for by melting of the assumed enriched mantle source, involving low-degree melting (~2%) in the garnet-facies followed by ~10% partial melting in the spinel-facies (dashed line in Fig. 16b). However, these melting conditions (dashed line in Fig. 16c) do not explain the Th-Nb composition of the studied basalts. Nonetheless, the hypothesis that the Balagne basalts were generated through polybaric melting cannot be ruled out. Finally, based on Nd isotopic signature, Renna et al. (2018) suggested that the Balagne primary melts may have been generated by a process of reactive melt migration within a lower crustal crystal mush.

Geological evidence from the crustal section of the ophiolites from Balagne Nappe and its correlation with the External Ligurian ophiolites.

The crustal section of the Navaccia Unit of the Balagne Nappe includes a thick sequence of pillow lava basalts, at least 700-800m thick. The collected data indicate that this sequence is affected by the same deformations of that of the sedimentary cover, which are mainly represented by west-verging folds cut by a system of strike-slip faults. Despite these deformations, the features of the pillow lava basalts as well as its relationship with the other components of the ophiolite sequence can still be fully reconstructed. A thin level of ophiolitic breccia has been found at the base of this sequence, whereas the top is characterized by a transition to the Chert Fm., which ranges in age from Callovian to Tithonian (De Wever et al., 1987; Peybernès et al., 2001). Sills of dolerite and basaltic dikes cut through the pillow lava basalts, which are topped by a level of pillow breccia. In addition, an intercalation of silts and silty sandstones with arkosic composition has been found at the uppermost part of the pillow lava sequence. This intercalation can be correlated with that described by Durand-Delga et al. (1997) at Piana di Castifao. This occurrence contains zircons derived from calc-alkaline granitoids of Hercynian Corsica, as well as fragments of micaschists, rhyolites, basalts, and Jurassic limestones, as reported by Durand-Delga et al. (1997).

The most notable feature of this crustal section, however, is the presence of debris derived from the European continental shelf at its base and within it. Also, the overlying sedimentary cover is characterized by abundant continental debris, suggesting that the ophiolites of the Balagne Nappe originated in an area of the Ligurian-Piedmont Oceanic Basin close to the ocean-continent transition of the Europe plate (Durand-Delga et al., 1997; Marroni and Pandolfi, 2007; Rossi et al., 2009). The characteristics of the Navaccia pillow lava section, coupled with its relevant thickness, allow the ophiolites from the Balagne Nappe to be correlated with those of the western External Ligurian Units. These ophiolites occur as slide blocks within a sedimentary mélange but their pristine relationships with the continental rocks have been clearly assessed (Marroni et al., 1998). In particular, the pillow lava basalts show primary relationships with continental granitoids of Late Carboniferous-Permian age (Di Rosa et al., 2024). The ophiolites in the western External Ligurian Units, such as those in the Balagne Nappe, are therefore thought to have originated from the ocean-continent transition, but on the opposite side of the Ligurian-Piedmont Oceanic Basin, specifically, the side of the Adria plate (Marroni et al., 1998; Marroni and Pandolfi, 2007; Montanini et al., 2008). Given their origin, the pillow lava basalts from both the Balagne Nappe and the External Ligurian Units are the oldest, having formed during the initial stage of spreading in the Ligurian-Piedmont oceanic basin, as depicted in the Fig. 17. Notably, both are characterized by the significant thickness of their pillow lava basalt sequences. This figure also postulates the interference in the Middle Jurassic between volcanic activity and siliciclastic sedimentation supplied by the continental margin of Europe plate.

CONCLUSIONS

The Balagne Nappe in north-western Corsica contains best-preserved ophiolitic sequences derived from the OCTZ of the Ligurian-Piedmont oceanic basin, making it a key area for reconstructing Alpine-Apennine oceanic evolution. Within this nappe, the Navaccia Unit exposes an exceptionally thick (700-800 m) and well-preserved succession of pillow-lava basalts. This volcanic sequence overlies ophiolitic breccias and is capped by Jurassic cherts, and it is intruded by dolerite sills and basaltic dikes. Arkosic sedimentary layers containing continental-derived debris are interlayered within the pillow lava pile.

Geochemically, the Navaccia pillow lavas consist mainly of tholeiitic basalts, with minor basaltic andesites (SiO_2 48-55 wt%) having a N-MORB general chemistry but showing clear enrichment in several incompatible elements. In particular, they are enriched in Ti, Nb, Th, Ta, Hf, and LREE compared with other basaltic rocks from Corsican ophiolitic and metaophiolitic units. Their chondrite-normalized REE patterns, characterized by strong depletion of HREE, indicate marked influence of residual garnet in the mantle source. Consistently, in the Dy/Yb vs. Ce/Yb discrimination diagram of Saccani (2015), the Navaccia basalts fall in the field for garnet-influenced basalts like those formed at the ocean-continent transition zone. Moreover, the hump-shaped LREE patterns, with $(La/Nd)_N$ ratios of 0.64-0.93, point to source heterogeneity. Semi-quantitative petrogenetic modelling of Ce, Dy, Yb, Th, and Nb suggests that the primary magmas formed through 8-12% partial melting of an enriched spinel-facies mantle component, combined with 5-10% melting of a garnet-pyroxenite source.

The thickness and good preservation of the Navaccia pillow lavas make this unit a natural laboratory for applying a chemostratigraphic study to better understand ocean-floor volcanism at the OCTZ of the Ligurian-Piedmont basin. This study shows a remarkable uniformity in incompatible elements contents and Mg# along the sequence, suggesting that the volcanic pile was built by repeated small eruptions that tapped magmas with similar degrees of partial melting and fractional crystallization, likely controlled by stable magma chamber processes.

The presence of abundant continental debris at the base and within the volcanic sequence indicates formation close to the European OCTZ of the Ligurian-Piedmont basin. Both stratigraphic architecture and geochemical characteristics of the Navaccia pillow lavas closely resemble those of ophiolites in the western External Ligurian Units, which formed at the opposite, Adria-side OCTZ. Together, these ophiolites represent some of the earliest volcanic products of the opening of the Ligurian-Piedmont oceanic basin.

ACKNOWLEDGEMENTS

Renzo Tassinari is kindly acknowledged for his help with XRF and ICP-MS analyses. Critical reviews by two anonymous reviewers helped to improve the manuscript. This work was financially supported by the University of Ferrara and the University of Pisa.

ONLINE SUPPLEMENTARY MATERIAL

Supplementary data to this article are available online at https://doi.org/10.4454/ofioliti.v52i1.592.

REFERENCES

Allègre C.J. and Minster J.F., 1978. Quantitative models of trace element behaviour in magmatic processes. Earth Planet. Sci. Letters, 38: 1-25.

Amann M., Ulrich M., Manatschal G., Pelt E., Epin M.E., Autin J. and Sauter D., 2020. Geochemical characteristics of basalts related to incipient oceanization: The example from the Alpine Tethys OCTs. Terra Nova. 32(1):75-88.

Barbero E., Delavari M., Dolati A., Vahedi L., Langone A., Marroni M., Pandolfi L., Zaccarini F. and Saccani E., 2020. Early Cretaceous Plume-Ridge Interaction Recorded in the Band-e-Zeyarat Ophiolite (North Makran, Iran): New Constraints from Petrological, Mineral Chemistry, and Geochronological Data. Minerals, 10: 1100; Doi:10.3390/min10121100.

Beccaluva L., Ohnenstetter D., Ohnenstetter M. and Venturelli G., 1977. The Trace Element Geochemistry of Corsican Ophiolites. Contrib. Mineral. Petrol., 64: 11-31.

Beccaluva L., DiGirolamo P., Macciotta G. and Morra V., 1983. Magma affinities and fractionation trends in ophiolites. Ofioliti 8: 307-324.

Bortolotti V., Principi G. and Treves B. 2001. Ophiolites, Ligurides and the tectonic evolution from spreading to convergence of a Mesozoic Western Tethys segment. In: Vai G.B. and Martini I.P. (Eds.) Anatomy of an Orogen: The Apennines and adjacent Mediterranean basins. Dordrecht Springer, Netherlands: 151-164.

Bortolotti V. and Principi G., 2005. Tethyan ophiolites and Pangea break-up. The Island Arc, 14: 442-470. Doi: 10.1111/j.1440-1738.2005.00491.x

Caron, J. M., and Péquignot, G. 1986. The transition between blueschists and lawsonite-bearing eclogites based on observations from Corsican metabasalts. Lithos, 19: 205-218.

Caron J., 1994. Metamorphism and deformation in Alpine Corsica. Schweiz. Mineral. Petrograph. Mitt., 74: 105-114

Chalot-Prat, F. (2005). An undeformed ophiolite in the Alps: Field and geochemical evidence for a link between volcanism and shallow plate tectonic processes. In: Foulger, G. R., Natland, J. H., Presnall, D. C. & Anderson, D. L. (eds) Plates, Plumes, and Paradigms: Geological Society of America, Special Papers 388, 751-780. Doi: 10.1130/0-8137-2388-4.751

Dal Piaz G.V. et al., 1977. I complessi ofiolitici e le unità cristalline della Corsica alpina. Ofioliti, 2: 265-324.

Decandia F.A. and Elter P., 1972. La zona ofiolitifera del Bracco nel settore compreso tra Levanto e la Val Graveglia (Appennino Ligure). Mem. Soc. Geol. It., 11: 503-530.

De Cesari F., Di Rosa M., Sanità E., Pandolfi L. and Marroni M., 2025. Long-lived sedimentation in the Western Tethys oceanic basin: revisiting the metasediments of Bagliacone-Riventosa Formation (Corsica, France). Int. Geol. Rev. Doi: 10.1080/00206814.2024.2411537.

De Wever P., Danelian T., Durand-Delga M., Cordey F. and Kito N., 1987. Datations des radiolarites post-ophiolitiques de Corse alpine à l'aide des radiolaires, C. R. Acad. Sci. Paris, série II, 305: 893-900.

Dilek Y. and Furnes H., 2019. Tethyan ophiolites and Tethyan seaways. Jour. Geol. Soc. London, 10, Doi: 10.1144/jgs2019-112.

Di Rosa M., Farina F., Marroni M., Heejin J. and Pandolfi L., 2024. U-PB ages from felsic rocks of the External Ligurian sedimentary mélange (Northern Apennine, Italy): tracing the pre-Jurassic history of the hyperextended Adria continental margin. Jour. Geol. Soc. London, 181, Doi: 10.1144/jgs2023-121.

Di Rosa M., Sanità E., Malasoma A., Pandolfi L. and Marroni M., 2025. Switching from contractional to extensional tectonics along the Alpine Front: structural and metamorphic evidence from the Balagne area (northern Corsica, France). Jour. Struct. Geol., 105471. Doi:10.1016/j.jsg.2025.105471.

Durand-Delga M., 1984. Principaux traits de la Corse Alpine et corrélations avec les Alpes Ligures. Mem. Soc. geol. it., 28: 285-329.

Durand-Delga M., Peybernès B. and Rossi P., 1997. Arguments en faveur de la position, au Jurassique, des ophiolites de Balagne (Haute-Corse, France) au voisinage de la marge continentale européenne. C. R. Acad. Sci. Paris, 32: 973-998.

Durand-Delga M., Fondecave-Wallez M.J. and Rossi P., 2005. L'unité ophiolitique de Pineto (Corse): signification du détritisme continental dans sa couverture de flysch albo-cénomanien. C. R. Géoscience, 337: 1084-1095. Doi: 10.1016/j.crte.2005.06.008.
Egal E., 1992. Structures and tectonic evolution of the external zone of Alpine Corsica. Jour. Struct. Geol., 14: 1215-1228. Doi: 10.1016/0191-8141(92)90071-4
Elter P., Grasso M., Parotto M. and Vezzani L., 2003. Structural setting of the Apennine-Maghrebian thrust belt. Episodes, 26: 205-211. Doi: 10.18814/epiiugs/2003/v26i3/010
Ewart A. and Griffin W.L., 1994. Application of Proton-Microprobe Data to Trace-Element Partitioning in Volcanic-Rocks. Chemical Geology, 117: 251-284. Doi: 10.1016/0009-2541(94)90131-7.
Flower M.F.J., Ohnmacht W., Robinson P.T., Schmincke H.-U. and Marfiner G., 1980. Lithologicand chemical stratigraphy at DSDP Sites 417 and 418. Initial rep. Deep Sea Drill. Proj., 51-53: 939-956.
Grove T.L. and Bryan W.B., 1983. Fractionation of pyroxene-phyric MORB at low pressure: An experimental study. Contrib. Mineral. Petrol., 84: 293-309.
Hofmann A.W., 1988. Chemical differentiation of the Earth: The relationship between mantle, continental crust, and oceanic crust. Earth Planet Sci. Letters, 90: 297-314.
Joron J.L. and Treuil M., 1989. Hygromagmaphile element distribution in oceanic basalts as fingerprints of partial melting and mantle heterogeneity: a specific approach and proposal of an identification of a modelling method. Magmatism in ocean Basins. In: Saunders A.D. and Norry M.J. (Eds.) Magmatism in the Ocean Basins. Geol. Soc. London Sp. Publ., 42: 277-299. Doi: 10.1144/gsl.sp.1989.042.01.17
Kinzler R.J., 1997. Melting of mantle peridotite at pressures approaching the spinel to garnet transition: application to mid-ocean ridge basalt petrogenesis. Jour. Geophys. Res., 102: 853-874.
Klein E.M. and Langmuir C.H., 1987. Global correlations of ocean ridge basalt chemistry with axial depth and crustal thickness. Jour. Geophys. Res., 92, No. B8: 8089-8115.
Lachance G.R. and Trail R.J., 1966. Practical solution to the matrix problem in X-ray analysis. Canadian Spectroscopy, 11: 43-48.
Lahondère D. and Guerrot C., 1997. Sm-Nd dating of Alpine eclogitic metamorphism in Corsica: evidence for Late Cretaceous subduction beneath the Corsican-Sardinian block. Géologie de la France, 3: 3-11.
Langmuir C.H., Klein E.M. and Plank T., 1992. Petrological systematics of mid-ocean ridge basalts: Constraints on melt generation beneath ocean ridges. In: Phipps Morgan J., Blackman D.K., Sinton J.M. (Eds.) Mantle Flow and Melt Generation at Mid-Ocean Ridges, Geophysical Monograph Series, 71: 183-280.
Levi N., Malasoma A., Marroni M., Pandolfi L. and Paperini M., 2007. Tectono-metamorphic history of the ophiolitic Lento unit (northern Corsica): evidence for the complexity of accretion-exhumation processes in a fossil subduction system. Geodinamica Acta, 20: 99-118. Doi: 10.3166/ga.20.99-118
Liu C.-Z., Snow J. E. and Hellebrand E., 2005. Geochemistry and petrology of a suite of garnet pyroxenites from ODP Leg 209: Implications for the origin of the MAR lithosphere. Earth Planet. Sci. Letters, 240: 539-553. Doi: 10.1016/j.epsl.2005.
Manatschal G. and Müntener O., 2009. A type sequence across an ancient magma-poor ocean–continent transition: the example of the western Alpine Tethys ophiolites. Tectonophysics, 473 (1-2): 4-19. Doi: 10.1016/j.tecto.2008.07.021
Marino M., Monechi S. and Principi G., 1995. New calcareous nannofossil data on the Cretaceous-Eocene age of Corsica turbidites. Riv. it. Paleont. Strat., 101: 49-62.
Marroni M., Molli G., Montanini A. and Tribuzio R., 1998. The association of continental crust rocks with ophiolites in the Northern Apennines (Italy): implications for the continent-ocean transition in the Western Tethys. Tectonophysics, 292: 43-66.

Marroni M., Pandolfi L. and Perilli N., 2000. Calcareous nannofossil dating of the San Martino Formation from the Balagne ophiolite sequence (Alpine Corsica): comparison with the Palombini Shale of the Northern Apennine. Ofioliti 25: 147-155.

Marroni M., Molli G., Ottria G. and Pandolfi L., 2001. Tectono-sedimentary evolution of the External Liguride units (Northern Apennines, Italy): Insights in the pre-collisional history of a fossil ocean-continent transition zone. Geodinamica Acta, 14: 307-320. Doi: 10.1080/09853111.2001.11432453

Marroni M. and Pandolfi L., 2003. Deformation history of the ophiolite sequence from the Balagne Nappe, northern Corsica: insights in the tectonic evolution of the Alpine Corsica. Geol. Jour., 38: 67-83. Doi: 10.1002/gj.943

Marroni, M. and Pandolfi, L., 2007. The architecture of an incipient oceanic basin: a tentative reconstruction of the Jurassic Liguria-Piemonte basin along the Northern Apennines-Alpine Corsica transect. Int. J. Earth Sci. Doi: 10.1007/s00531-006-0163-x.

Marroni M., Meneghini F. and Pandolfi L., 2017. A revised subduction inception model to explain the Late Cretaceous, double-vergent orogen in the precollisional western Tethys: Evidence from the Northern Apennines. Tectonics, 36: 2227-2249. Doi: 10.1002/2017TC004627

McKenzie D. and O'Nions R.K., 1991. Partial melt distributions from inversion of rare Earth element concentrations. Jour. Petrol., 32: 1021-1091. Doi: 10.1093/petrology/32.5.102.

Meneghini F., Di Rosa M., Marroni M., Raimbourg H. and Pandolfi L., 2023. Subduction signature in the Internal Ligurian Units (Northern Apennine, Italy): evidence from P-T metamorphic peak estimate. Terra Nova, 36: 182-190. Doi: 10.1111/ter.12684

Meresse F., Lagabrielle Y., Malavieille J. and Ildefonse B., 2012, A fossil ocean-continent transition of the Mesozoic Tethys preserved in the Schistes Lustrés Nappe of northern Corsica: Tectonophysics, 579: 4-16. Doi: 10.1016/j.tecto.2012.03.025

Montanini A., Tribuzio R. and Vernia L., 2008. Petrogenesis of basalts and gabbros from an ancient continent-ocean transition (External Liguride ophiolites, Northern Italy). Lithos, 101: 453-479. Doi: 10.1016/j.lithos.2007.09.007

Nardi R. 1968. Le unità alloctone della Corsica e la loro correlazione con le unità delle Alpi e dell'Appennino. Mem. Soc. geol. it., 7: 323-344.

Nardi R., Puccinelli A. and Verani M., 1978. Carta geologica della Balagne "sedimentaria" (Corsica) alla scala 1:25.000 e note illustrative. Boll. Soc. geol. It., 97: 3-22.

Pandolfi L., Marroni M. and Malasoma A., 2016. Stratigraphic and structural features of the Bas-Ostriconi Unit (Corsica): paleogeographic implications. C. R. Géosciences, 348: 630-640. Doi: 10.1016/j.crte.2015.12.001

Pearce J.A. and Norry M.J., 1979. Petrogenetic implications of Ti, Zr, Y, and Nb variations in volcanic rocks. Contrib. Mineral. Petrol., 69: 33-47.

Pearce J.A., 1996. A user's guide to basalt discrimination diagrams. In: Bailes, A.H., Christiansen, E.H., Galley, A.G., Jenner, G.A., Keith, J.D., Kerrich, R., Wyman, D.A. (Eds.) Trace Element Geochemistry of Volcanic Rocks: Applications for Massive Sulphide Exploration. Short Course Notes. vol. 12. Geol. Ass. Canada: 79-113.

Pearce J.A., 2008. Geochemical fingerprinting of oceanic basalts with applications to ophiolite classification and the search for Archean oceanic crust. Lithos, 100: 14-48. Doi: 10.1016/j.lithos.2007.06.016

Peybernès B., Durand-Delga M., Rossi P. and Cugny P., 2001. Nouvelles datations micropaléontologiques dans les séquences intra- et post-ophiolitiques de la Nappe de Balagne (Corse) et essai de re-constitution d'un segment de la marge occidentale de l'océan liguro-piémontais. Eclogae geol. Helv. 94: 95-105.

Rampone E., Hofmann A.W. and Rackzek I., 1998. Isotopic constraints within the Internal Liguride ophiolites (N. Italy): The lack of a genetic mantle-crust link. Earth Planet. Sci. Lett. 163: 175-189.

Rampone E., Borghini G. and Basch V., 2020. Melt migration and melt-rock reaction in the Alpine-Apennine peridotites: Insights on mantle dynamics in extending lithosphere, Geosci. Front., 11, 151-166. Doi: 10.1016/j.gsf.2019.02.006

Rampone E. and Sanfilippo A., 2021. The heterogeneous Tethyan oceanic lithosphere of the Alpine ophiolites. Elements: An International Magazine of Mineralogy, Geochemistry, and Petrology: 17(1), 23-28. Doi: 10.2138/gselements.17.1.23

Renna M.R., Tribuzio R., Sanfilippo A. and Tiepolo M., 2017. Zircon U-Pb geochronology of lower crust and quartzo-feldspathic clastic sediments from the Balagne ophiolite (Corsica). Swiss Jour. Geosci., 110: 479-501. Doi: 10.1007/s00015-017-0260-9

Renna M.R., Tribuzio R., Sanfilippo A. and Thirlwall M., 2018. Role of melting process and melt-rock reaction in the formation of Jurassic MORB-type basalts (Alpine ophiolites). Contrib. Mineral. Petrol., 173: 31. Doi: 10.1007/s00410-018-1458-2

Rossi P., Durand-Delga M., Lahondère J-C. and Lahondère D., 2001. Notice explicative de la feuille Santo-Pietro-di-Tenda, Carte géologique de la France (1/50000), BRGM, Orléans, France.

Rossi P., Cocherie A., Lahondère D. and Fanning C.M., 2002. La marge européenne de la Téthys jurassique en Corse: datation de trondhjémites de Balagne et indices de croûte continentale sous le domaine Balano-Ligure. C. R. Acad. Sci. Paris Géoscience 334: 313-322.

Rossi P., Durand-Delga M., Lahondere J.C., Baud J.P., Egal E., Lahondere D., Laporte D., Lluch D., Loyle M.D., Ohnenstetter M. and Palagi P., 2009. Carte Géologique de France (1/50000), feuille Santo Pietro di Tenda (1106) BRGM, Orléans.

Rudnick R.L. and Fountain D.M., 1995. Nature and composition of the continental crust: A lower crustal perspective. Reviews of Geophysics, 33: 267-309.

Saccani E., 2015. A new method of discriminating different types of post-Archean ophiolitic basalts and their tectonic significance using Th-Nb and Ce-Dy-Yb systematics. Geoscience Frontiers, 6: 481--501. Doi: 10.1016/j.gsf.2014.03.006.

Saccani E., Principi G., Garfagnoli F. and Menna F., 2008. Corsica ophiolites: Geochemistry and petrogenesis of basaltic and metabasaltic rocks. Ofioliti, 33: 187-207.

Saccani E., Dilek Y., Marroni M. and Pandolfi L., 2015. Continental Margin Ophiolites of Neotethys: Remnants of Ancient Ocean-Continent Transition Zone (OCTZ) Lithosphere and Their Geochemistry, Mantle Sources and Melt Evolution Patterns. Episodes, 38: 230-249. Doi: 210.18814/epiiugs/12015/v18838i18814/82418.

Saccani E., Padoa E. and Tassinari R., 2000. Preliminary data on the Pineto gabbroic Massif and Nebbio basalts: progress toward the geochemical characterization of Alpine Corsica ophiolites. Ofioliti, 25: 75-85.

Sanità E. Lardeaux J.M., Marroni M. and Pandolfi L., 2022a. Kinematics of the Helminthoid Flysch-Marguareis Unit tectonic coupling: consequences for the tectonic evolution of Western Ligurian Alps. C. R. Géoscience, 354: 141-157. Doi: 10.5802/crgeos.124.

Sanità E., Di Rosa M., Lardeaux J.-M., Marroni M. and Pandolfi L., 2022b. The Moglio-Testico Unit (Ligurian Alps, Italy) as Subducted Metamorphic Oceanic Fragment: Stratigraphic, Structural and Metamorphic Constraints. Minerals, 12: 1343. Doi: 10.3390/min12111343

Sanità E., Di Rosa M., Lardeaux J.-M., Marroni M. and Pandolfi L., 2023. Tectonic coupling of oceanic and continental units in the Southwestern Alps (Western Liguria, Italy) revealed by structural mapping. Journal of Maps, *19*. Doi: 10.1080/17445647.2023.2214789.

Sanità E., Di Rosa M., Marroni M., Meneghini F. and Pandolfi L., 2024. Insights into the subduction of the Ligure-Piemontese oceanic basin: new constraints from the metamorphism in the Internal Ligurian Units (Northern Apennines, Italy). Minerals, 14: 64, Doi: 10.3390/min14010064.

Sanità E., Di Rosa M. and Mugnaioli E., 2025. Non-conventional pressure estimates by using transmission electron microscopy coupled with energy-dispersive spectroscopy (TEM-EDS):

testing on submicrometer white mica from low-grade metapelites. European Jour. Mineral., 37: 343-352. Doi: 10.5194/ejm-37-343-2025.

Shervais J.W., 1982. Ti-V plots and the petrogenesis of modern ophiolitic lavas. Earth Planet. Sci. Letters, 59: 101-118.

Stampfli G.M., Borel G.D., Marchant R. and Mosar J., 2002. Western Alps geological constraints on western Tethyan reconstruction. In: Rosenbaum, G. and Lister, G.S. (Eds.), reconstruction of the evolution of the Alpine-Himalayan orogen. Journal of the Virtual Explorer: 77-106. Doi: 10.3809/jvirtex.2002.00056

Stracke, A., Hofmann, A.W. and Hart, S.R., 2005. FOZO, HIMU, and the rest of the mantle zoo. Geochemistry, Geophysics, Geosystems, 6: Q05007. Doi: 10.1029/2004GC000824

Sun S.-S. and McDonough W.F., 1989. Chemical and isotopic systematics of ocean basalts: Implications for mantle composition and processes. In: Saunders A.D. and Norry M.J. (Eds.), Magmatism in the Ocean Basins. Geol. Soc. London Sp. Publ., 42: 313-346.

Treves B. and Harper G.D., 1994. Exposure of serpentinites on the ocean floor: sequence of faulting and hydrofracturing in the northern Apennine ophicalcites. Ofioliti, 19b: 435-466.

Tribuzio R., Tiepolo M. and Vannucci R., 2000. Evolution of gabbroic rocks of the Northern Apennine ophiolites (Italy): Comparison with the lower oceanic crust from modern slow-spreading ridges. In: Dilek Y., Moores E.M., Elthon D. and Nicolas A. (eds), Ophiolites and Oceanic Crust: New Insights from Field Studies and the Ocean Drilling Program. Geol. Soc. Am. Spec. Pap., 349: 129–152. Doi: 10.1130/0-8137-2349-3.129.

Venturelli G., Capedri S., Thorpe R.S. and Potts P.J., 1979. Rare-earth and other trace element distribution in some ophiolitic metabasalts of Corsica. Chem. Geol., 24: 339-353.

Vidal O. and Parra T., 2000. Exhumation paths of high-pressure metapelites obtained from local equilibria for chlorite-phengite assemblage. Geol. Jour., 35: 139-161. Doi: 10.1002/1099-1034(200007/09)35:3/4<139::AID-GJ846>3.0.CO;2-0

Waters C.N., 1990. The Cenozoic tectonic evolution of Alpine Corsica. Geol. Soc. London Sp. Publ., 147: 811-824. Doi: 10.1144/GSL.SP.1989.045.01.43

Workman R.K. and Hart S.R., 2005. Major and trace element composition of the depleted MORB mantle (DMM). Earth Planet. Sci. Letters, 231: 53-72. Doi: 10.1016/j.epsl.2004.12.005

Winchester J.A. and Floyd P.A., 1977. Geochemical discrimination of different magma series and their differentiation products using immobile elements. Chem. Geol., 20: 325-343. Doi: 10.1016/0009-2541(77)90057-2

Xu Y.G., 2002. Evidence for crustal components in the mantle and constraints on crustal recycling mechanisms: pyroxenite xenoliths from Hannuoba, North China. Chem. Geol., 182: 301-322. Doi: 10.1016/S0009-2541(01)00297-6

Zanzucchi P., Sanità E., Catanzariti R., Pandolf L. and Marroni, M., 2025. Revisiting the Internal Ligurian Units of the Antessio area (Ligurian Apennines, Italy): insights into the oceanic lithosphere of the Liguria. Ofioliti, 50: 47-62. Doi: 10.4454/ofioliti.v50i1.590

Zhang G., Zeng Z.; Yin X., Wang X. and Chen D., 2009. Deep Fractionation of Clinopyroxene in the East Pacific Rise 13°N: Evidence from High MgO MORB and Melt Inclusions. Acta Geologica Sinica, 83: 266-277. Doi: 10.1111/j.1755-6724.2009.00023.x

Zindler A. and Hart S., 1986. Chemical geodynamics. Annual Review of Earth and Planetary Sciences, 14: 493-571. Doi: 10.1146/annurev.ea.14.050186.002425

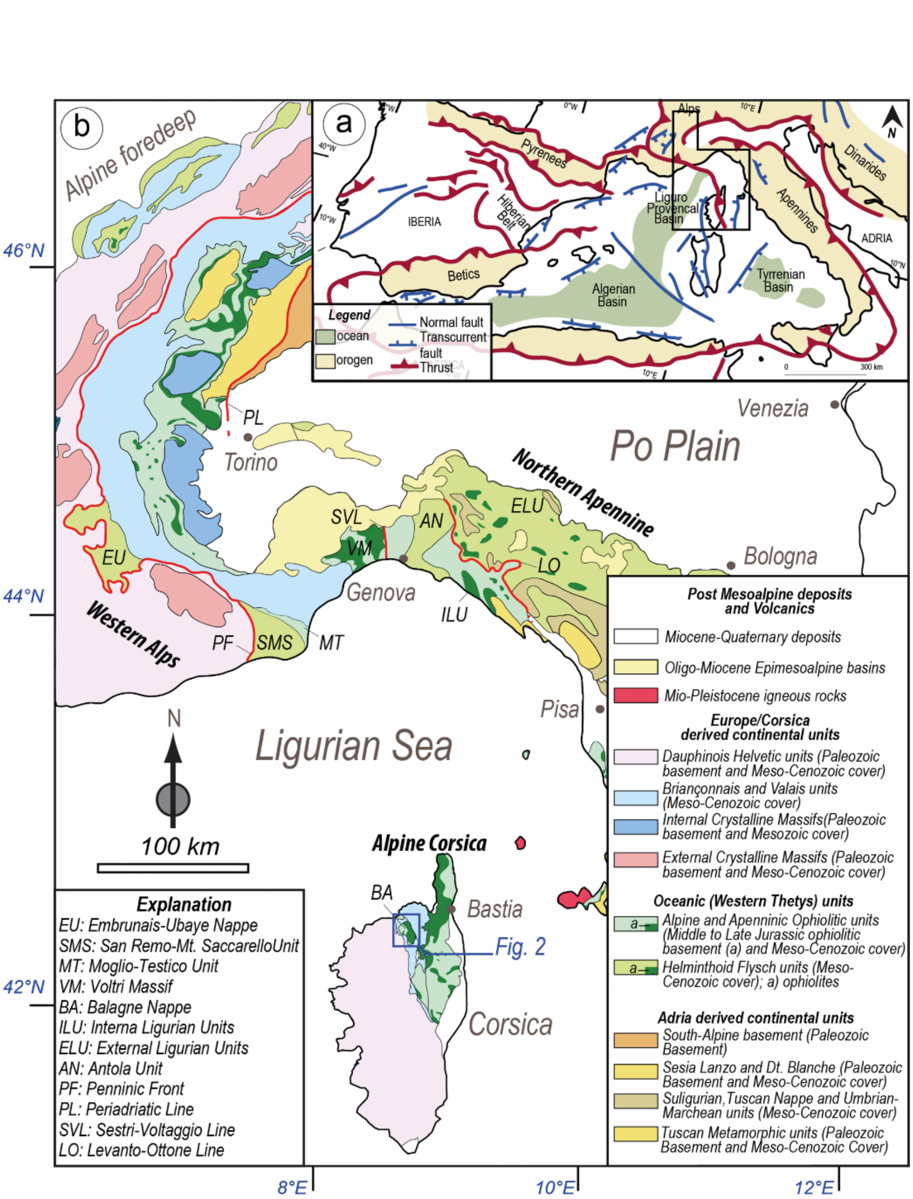

Fig. 1 - (a) Location of the Fig. 1b within the geological framework of the Western Mediterranean (modified from Marroni et al., 2017); (b) Tectonic setting of the Western Alps, the Northern Apennines and Corsica (modified from Di Rosa et al., 2024). The location of the Fig. 2 is indicated.

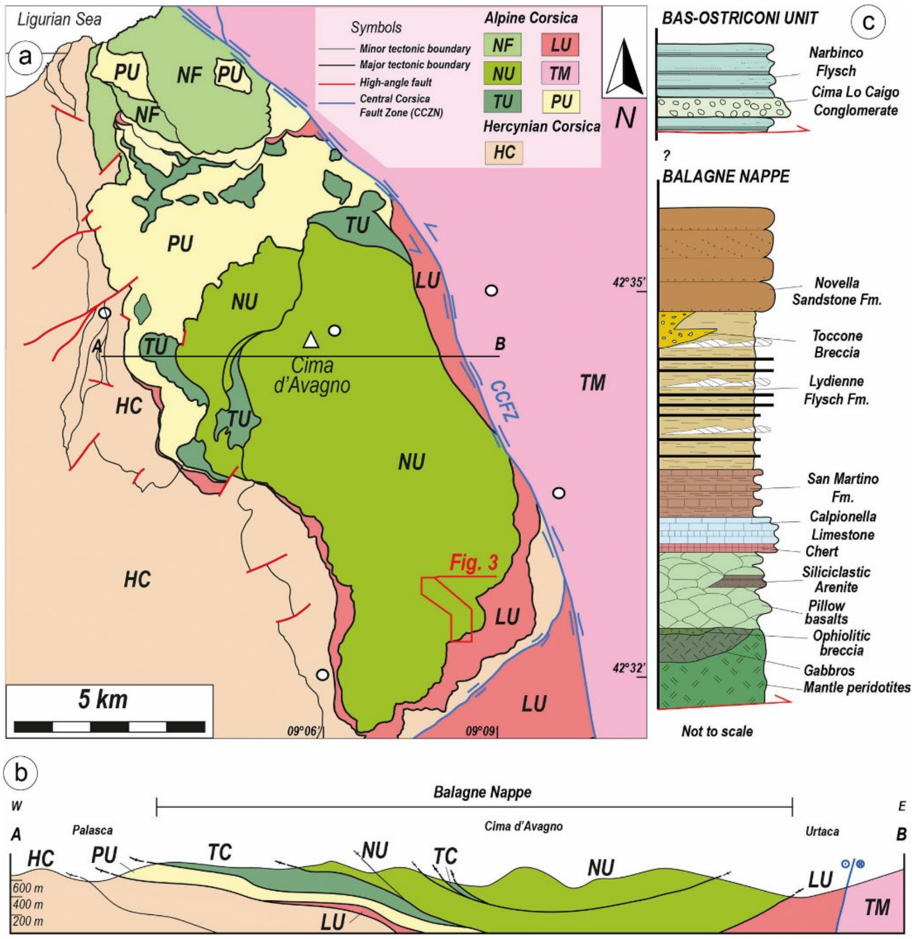

Fig. 2 - (a) Tectonic sketch map of the Balagne area (modified from Marroni and Pandolfi, 2003). Line A-B shows the trace of the geological cross section in Fig. 2b. The area depicted in the Fig.3 is also indicated; (b) East-West trending geological cross section of the Balagne area; c) Reconstructed logs of the Balagne Nappe and the Bas-Ostriconi Unit.

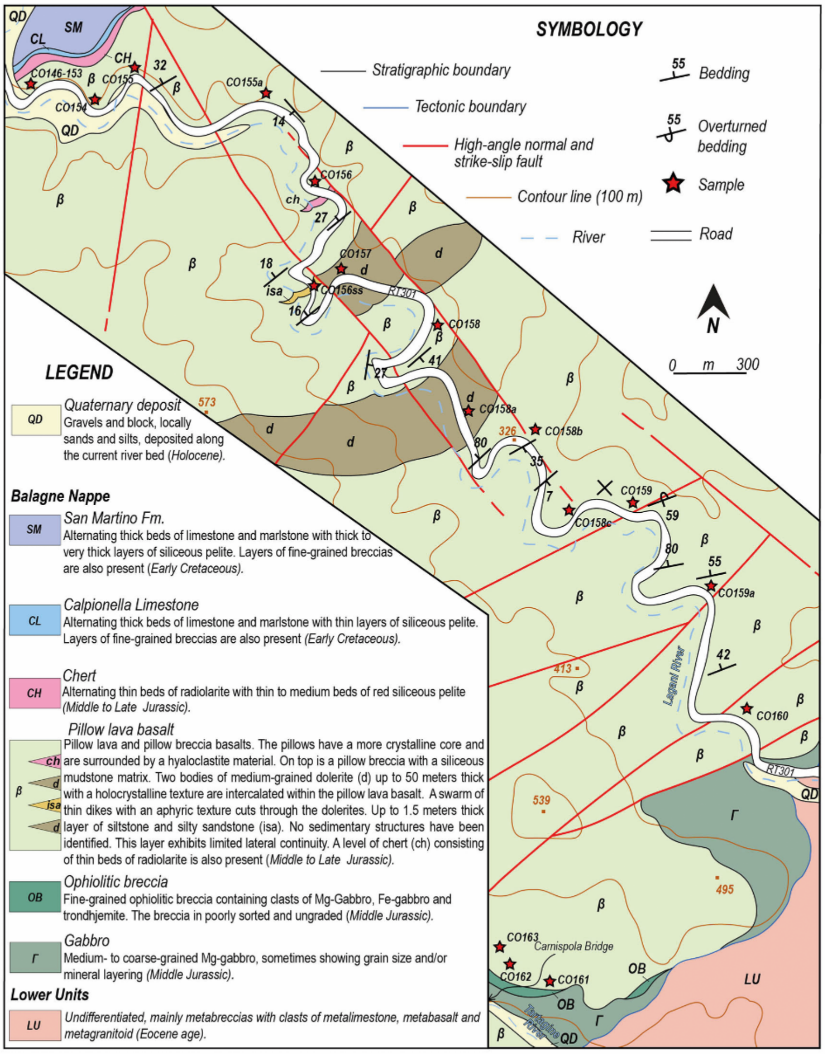

Fig. 3 - Geological map of the Lagani Valley. The location of the collected samples is indicated.

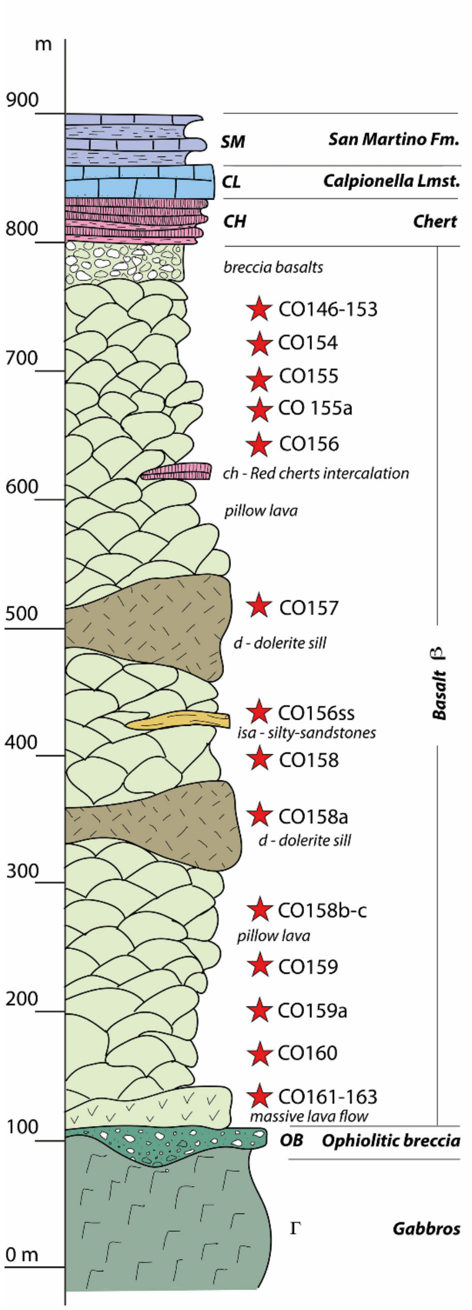

Fig. 4 - Stratigraphic log of the ophiolite sequence reconstructed in the Lagani Valley. The position of the collected samples is indicated.

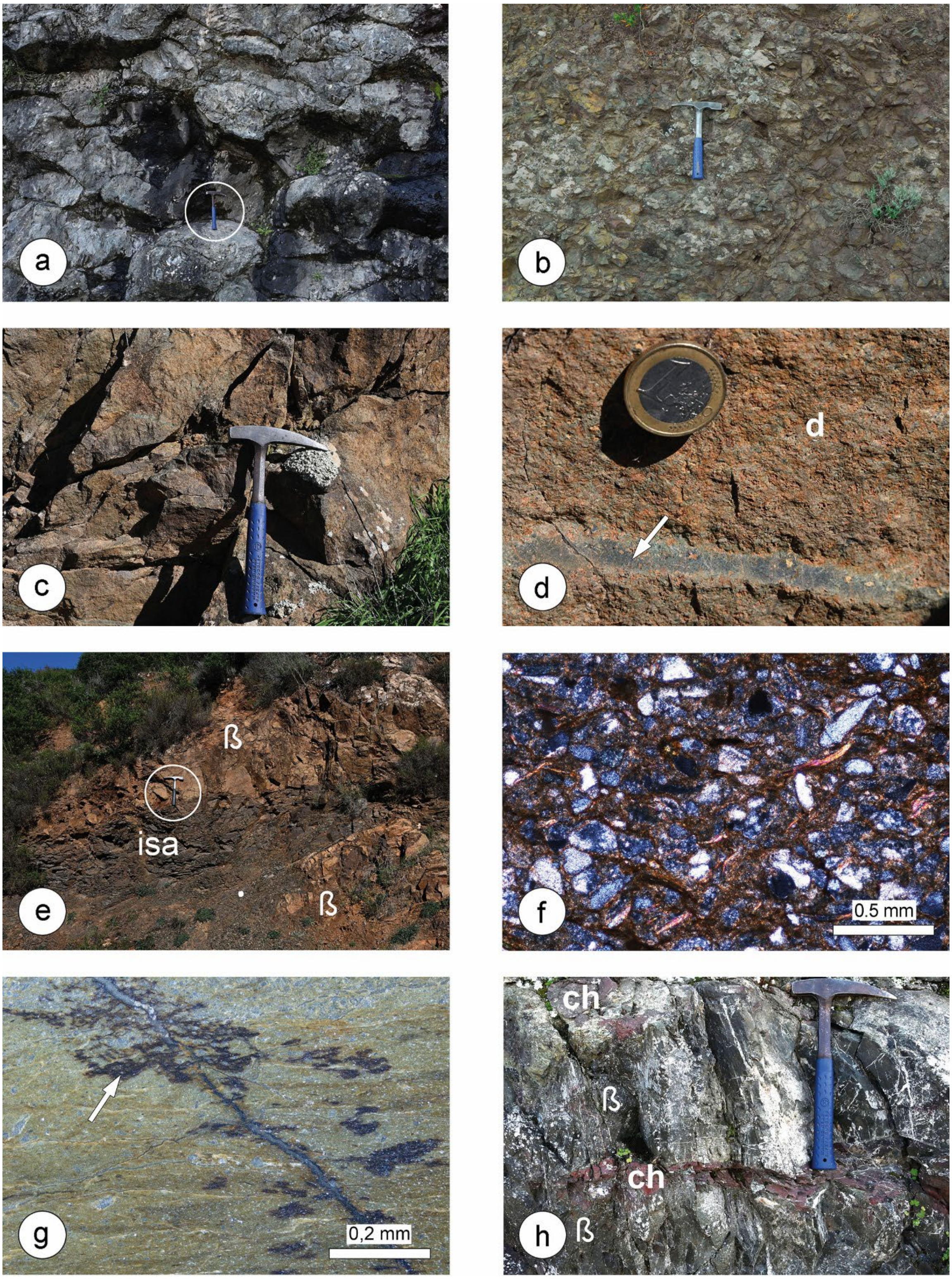

Fig. 5 - Meso- and microscale features of the Lagani Valley sequence. (a) Pillow lava basalts; (b) Pillow lava breccia; (c) field occurrence of the dolerites; (d) small dike of aphyric basalt within the dolerites; (e) layer of siltstones and silty-sandstones (isa) within the pillow lavas (b); (f) microscale features of the-silty sandstones, crossed-pols; (g) trace of bioturbation (arrow) in the siltstones (isa) within the pillow lavas; (h) Intercalation of red cherts (ch) within the pillow lava basalts (b).

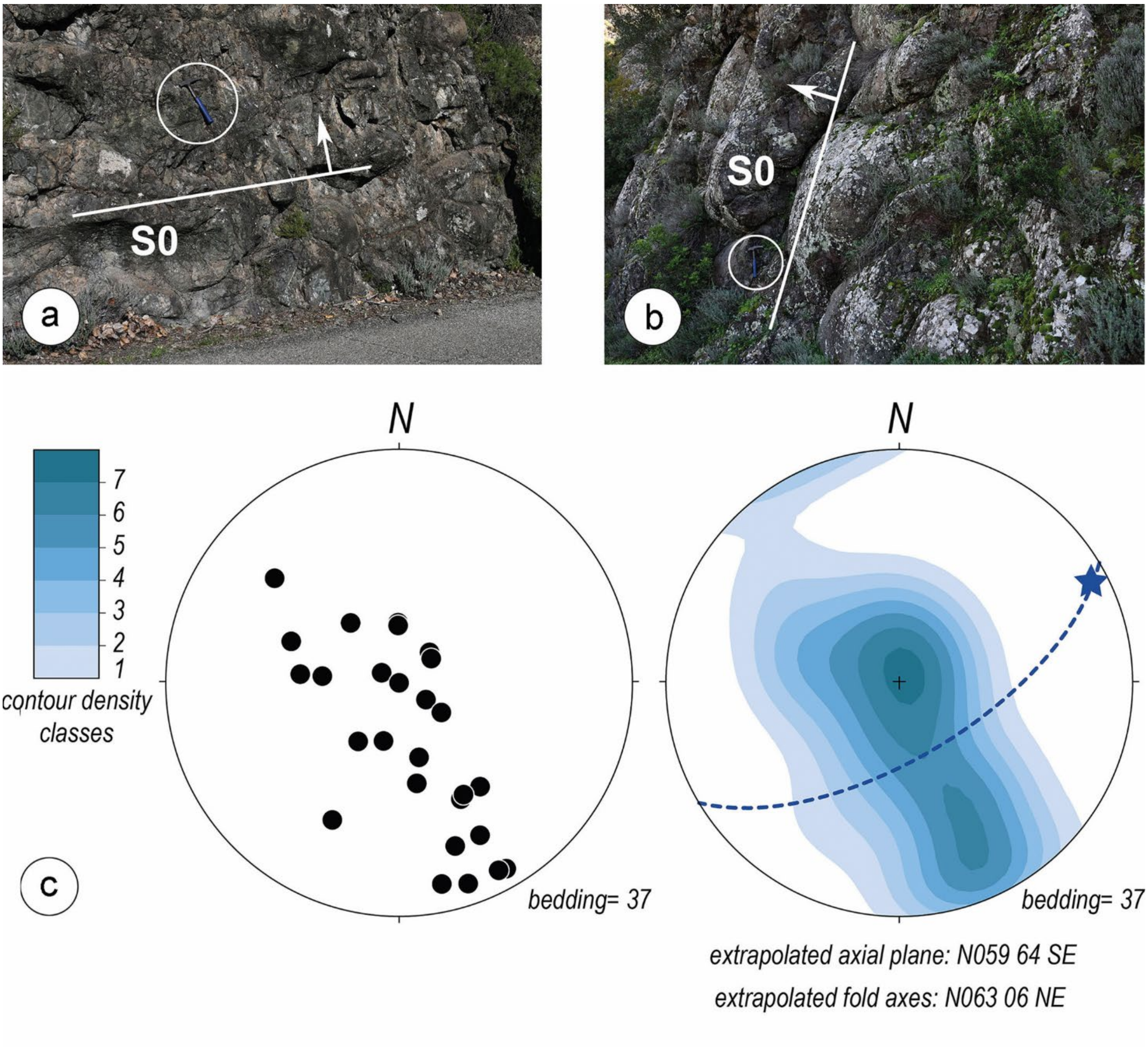

Fig. 6 - Deformations of the pillow lava basalts. (a) horizontal pillows; (b) almost vertical pillows; (c) stereographic plot of the pillows attitude and contouring of the pillows attitude; Schmidt net, equal area, lower hemisphere stereographic representation.

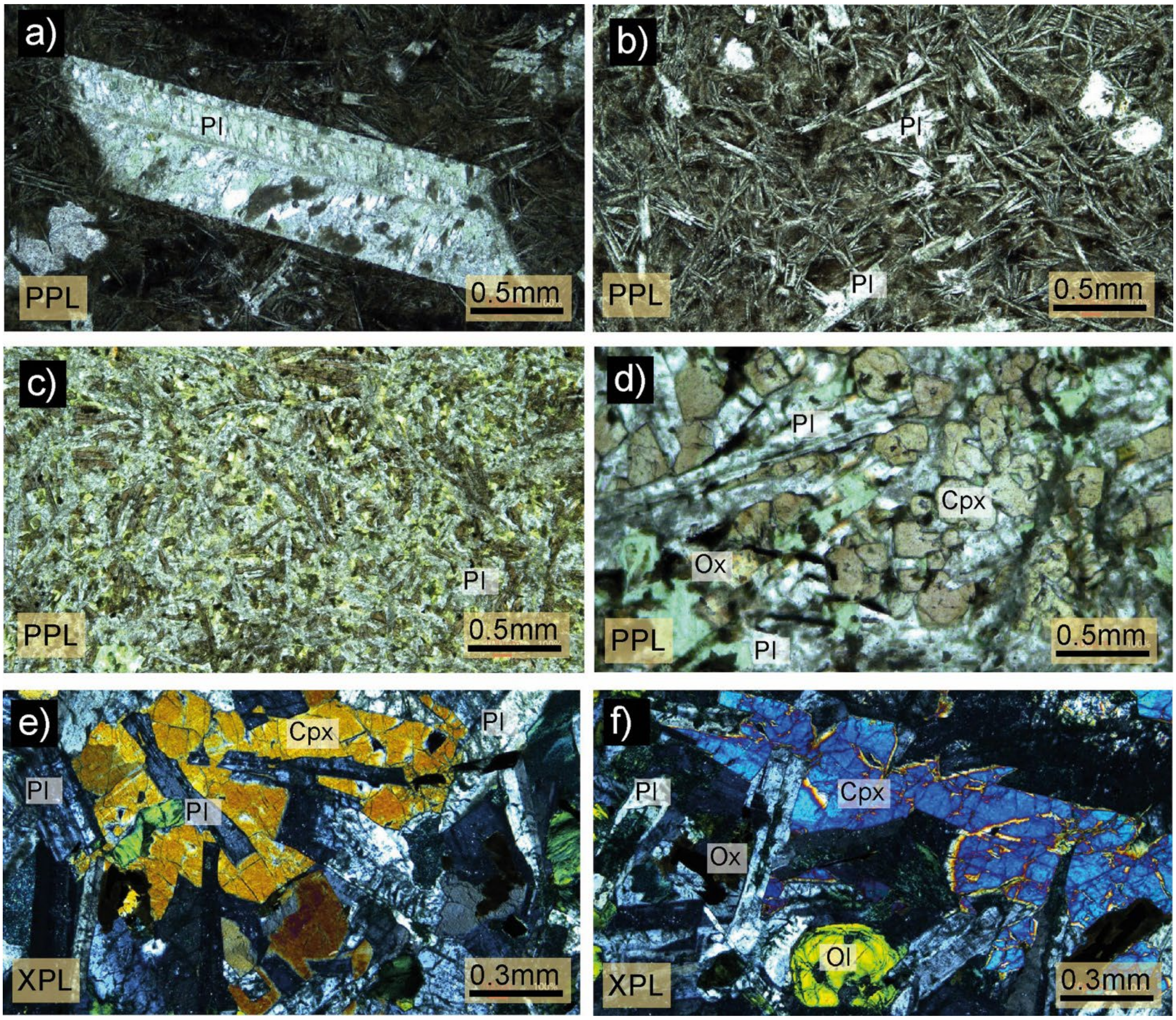

Fig. 7 - Microphotos showing the main textures and mineral phases in the Navaccia pillow lavas. Abbreviations. PPL: plane polarized light; XPL: crossed polarized light; Pl: plagioclase; Cpx: clinopyroxene; Ol: olivine; Ox: Fe-Ti-oxides. (a) basalt CO151; (b) basaltic andesite CO148; (c) basalt CO153; (d) basalt CO155a; (e) doleritic dyke CO158a; (f) doleritic dyke CO158.

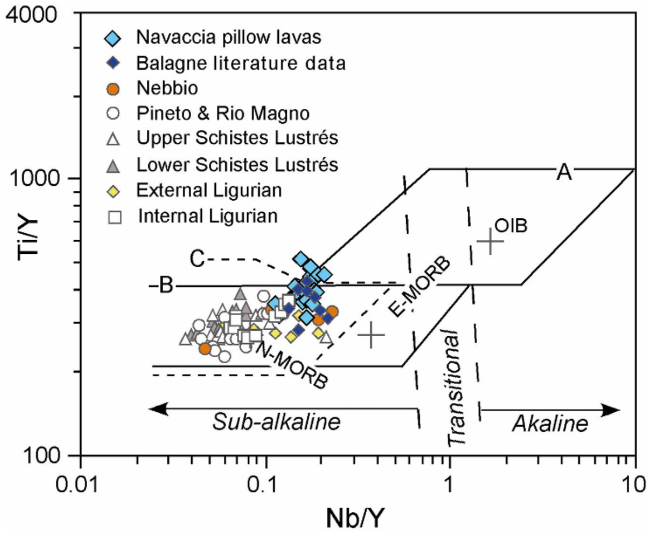

Fig. 8 - Nb/Y vs. Ti/Y discrimination diagram of Winchester and Floyd (1977) modified by Pearce (1996) for volcanic rocks and sills from the Navaccia pillow lavas. The compositions of basaltic rocks from various ophiolitic and metaophiolitic units of the Alpine Corsica and both External and Internal Ligurian units of the Northern Apennine are shown for comparison (data from Durand-Delga et al., 1997; Rampone et al., 1998; Saccani et al., 2000, 2008; Montanini et al., 2008; Renna et al., 2018). Grey crosses show the compositions of typical normal-type mid-ocean ridge basalt (N-MORB) and enriched-type mid-ocean ridge basalt (E-MORB); data from Sun and McDonough (1989). Abbreviations, N-MORB: normal-type mid-ocean ridge basalt; E-MORB: enriched-type mid-ocean ridge basalt; OIB: alkaline oceanic within-plate basalt. Compositional fields for alkaline ocean island basalts (A), Mid-ocean ridge basalts (B), and calc-alkaline basalts (C) are from Pearce (1996).

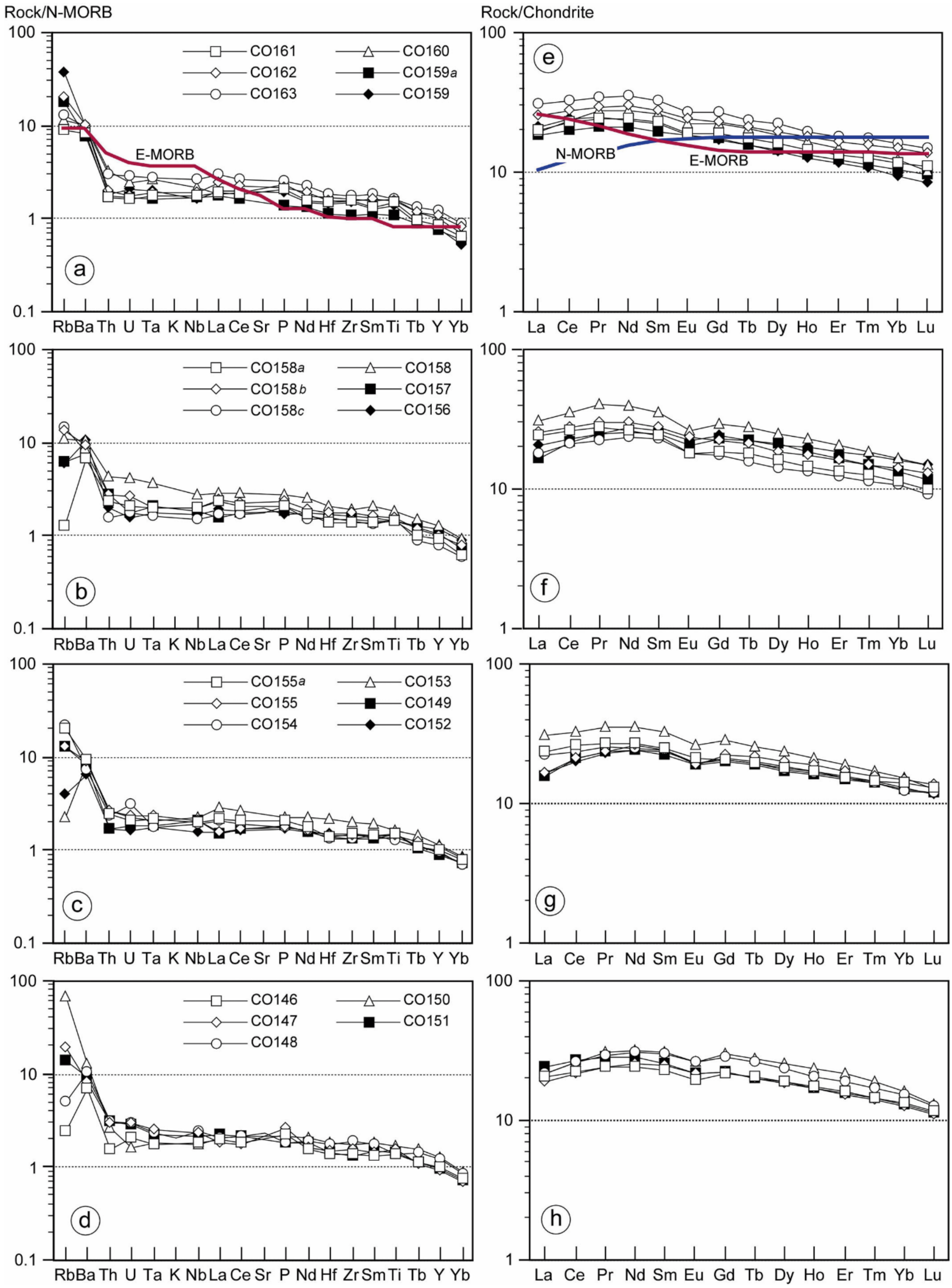

Fig. 9 - N-MORB normalized incompatible element patterns (a-d) and chondrite-normalized REE patterns (e-h) for volcanic rocks and sills from the Navaccia pillow lavas. Normalizing values are from Sun and McDonough (1989). Patterns for the typical normal-type mid-ocean ridge basalt (N-MORB) and enriched-type mid-ocean ridge basalt (E-MORB) are show in Panels a) and e) (data from Sun and McDonough, 1989).

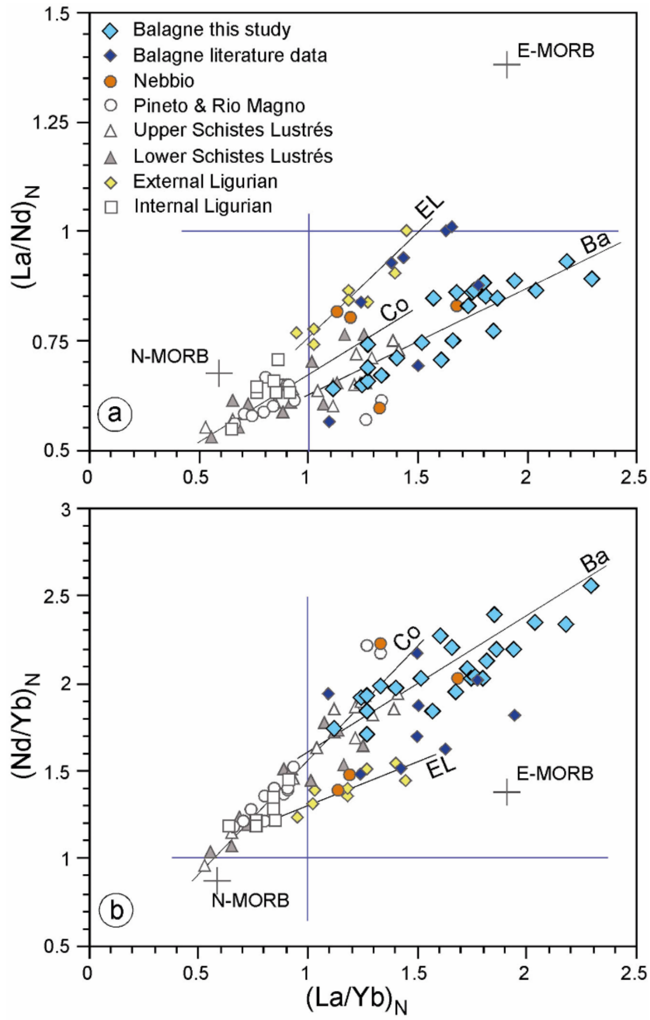

Fig. 10 - Chondrite-normalized (La/Nd) vs. (La/Yb) (a) and (Nd/Yb) vs. (La/Yb) (b) diagrams for volcanic rocks and sills from the Navaccia pillow lavas. Normalizing values and the compositions of typical normal-type mid-ocean ridge basalt (N-MORB) and enriched-type mid-ocean ridge basalt (E-MORB) are shown with grey crosses; data from Sun and McDonough (1989). The compositions of basaltic rocks from various ophiolitic and metaophiolitic units of the Alpine Corsica and both External and Internal Ligurian Units of the Northern Apennine are shown for comparison (data from Durand-Delga et al., 1997; Rampone et al., 1998; Saccani et al., 2000, 2008; Montanini et al., 2008; Renna et al., 2018). Light blue lines represent the REE ratios = 1; black lines represent the rough compositional trends of the Balagne basalts (Ba), Corsica basaltic and metabasaltic rocks (Co), and External Ligurian basalts (EL).

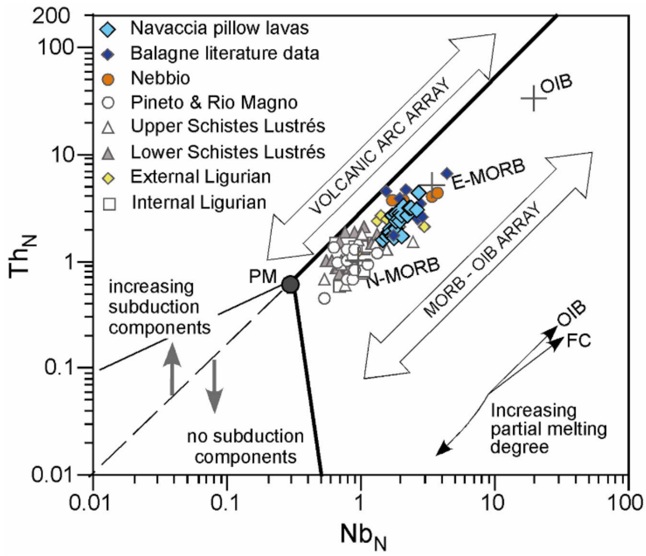

Fig. 11 - N-MORB normalized Th vs. Nb discrimination diagram of Saccani (2015) for volcanic rocks and sills from the Navaccia pillow lavas. Vectors indicate the trends of compositional variations due to the main petrogenetic processes (OIB: ocean island, plume-type component enrichment; FC: fractional crystallization The compositions of basaltic rocks from various ophiolitic and metaophiolitic units of the Alpine Corsica and both External and Internal Ligurian (units of the Northern Apennine are shown for comparison (data from Durand-Delga et al., 1997; Rampone et al., 1998; Saccani et al., 2000, 2008; Montanini et al., 2008; Renna et al., 2018). Abbreviations, MORB: mid-ocean ridge basalt; N-: normal type; E-: enriched type; OIB: alkaline oceanic within-plate basalt. Normalizing values, as well as the composition of typical N-MORB, E-MORB, and OIB, show with gray crosses, are from Sun and McDonough (1989).

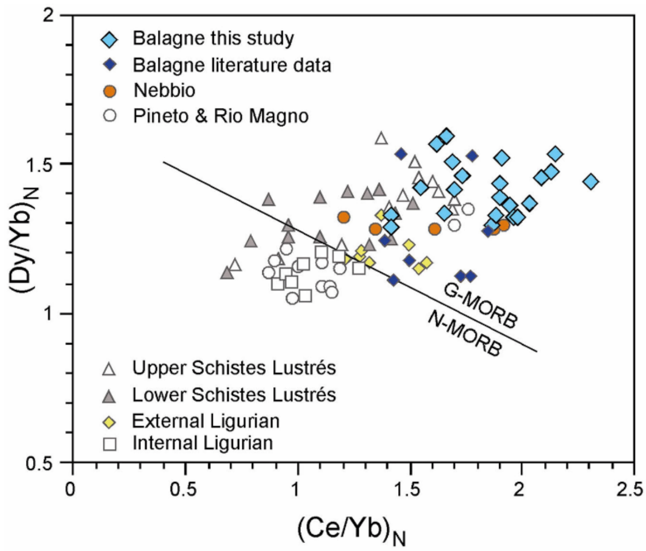

Fig. 12 - Chondrite-normalized (Sun and McDonough, 1989) Dy/Yb vs. Ce/Yb diagram of Saccani (2015) used for discriminating between garnet-influenced mid-ocean ridge basalts (G-MORB) and garnet-not influenced normal-type mid-ocean ridge basalts (N-MORB) for volcanic rocks and sills from the Navaccia pillow lavas. The compositions of basaltic rocks from various ophiolitic and metaophiolitic units of the Alpine Corsica and both External and Internal Ligurian units of the Northern Apennine are shown for comparison (data from Durand-Delga et al., 1997; Rampone et al., 1998; Saccani et al., 2000, 2008; Montanini et al., 2008; Renna et al., 2018).

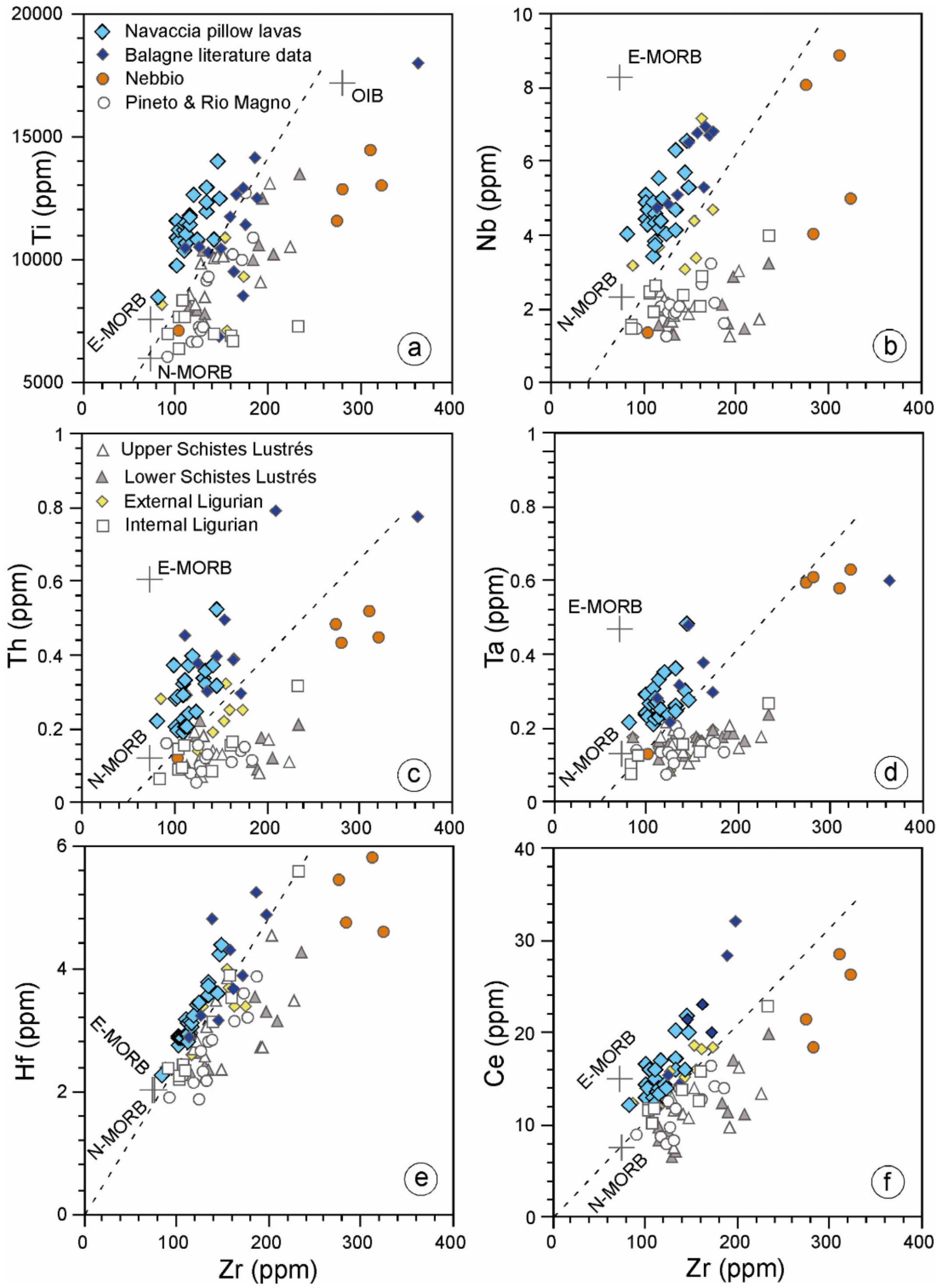

Fig. 13 - Variation of selected incompatible elements (in ppm) vs. Zr (in ppm) for volcanic rocks and sills from the Navaccia pillow lavas. The compositions of basaltic rocks from various ophiolitic and metaophiolitic units of the Alpine Corsica and both External Ligurian and Internal Units of the Northern Apennines are shown for comparison (data from Durand-Delga et al., 1997; Rampone et al., 1998; Saccani et al., 2000, 2008; Montanini et al., 2008 Renna et al., 2018). Grey crosses show the composition of typical normal-type mid-ocean ridge basalt (N-MORB), enriched-type mid-ocean ridge basalt (E-MORB), and alkaline oceanic within-plate basalt (OIB); data from Sun and McDonough (1989). N-MORB, E-MORB, and alkaline oceanic within-plate basalt. are from Sun and McDonough (1989). The dashed lines roughly mark the compositional differences between the Balagne basaltic rocks and their equivalents from Corsica and External Ligurian ophiolitic and metaophiolitic units. Legend is split in panels a) and c).

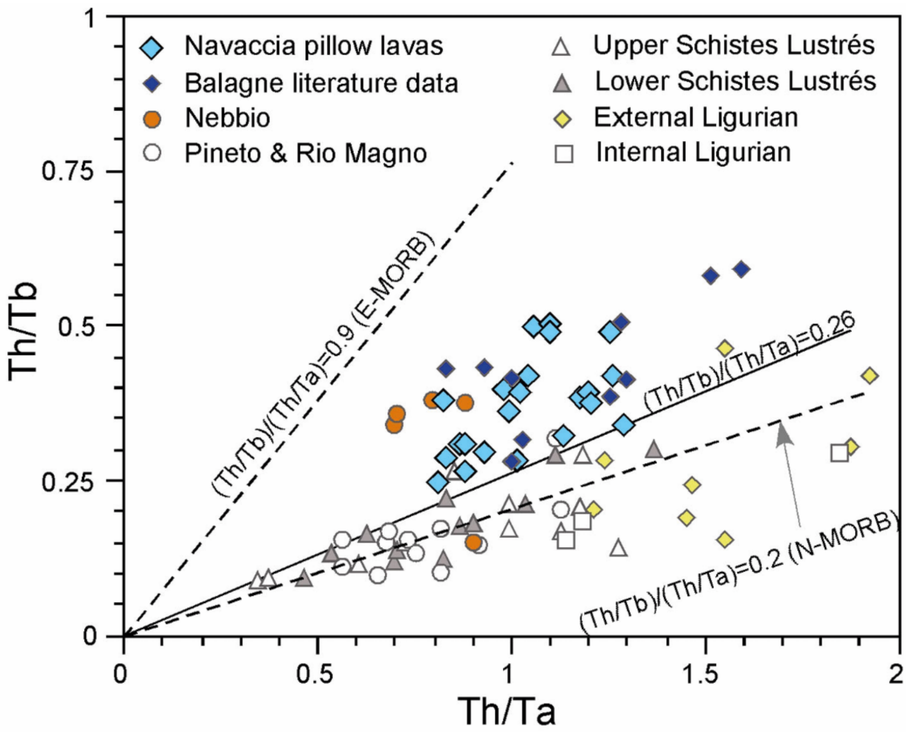

Fig. 14 - Th/Tb vs. Th/Ta diagram for volcanic rocks and sills from the Navaccia pillow lavas. The compositions of basaltic rocks from various ophiolitic and metaophiolitic units of the Alpine Corsica and both External and Internal Ligurian Units of the Northern Apennines are shown for comparison (data from Durand-Delga et al., 1997; Rampone et al., 1998; Saccani et al., 2000, 2008; Montanini et al., 2008 Renna et al., 2018). Dashed lines represent (Th/Tb)/(Th/Ta) ratios for typical normal-type mid-ocean ridge basalt (N-MORB) and enriched-type mid-ocean ridge basalt (E-MORB); data from Sun and McDonough (1989).

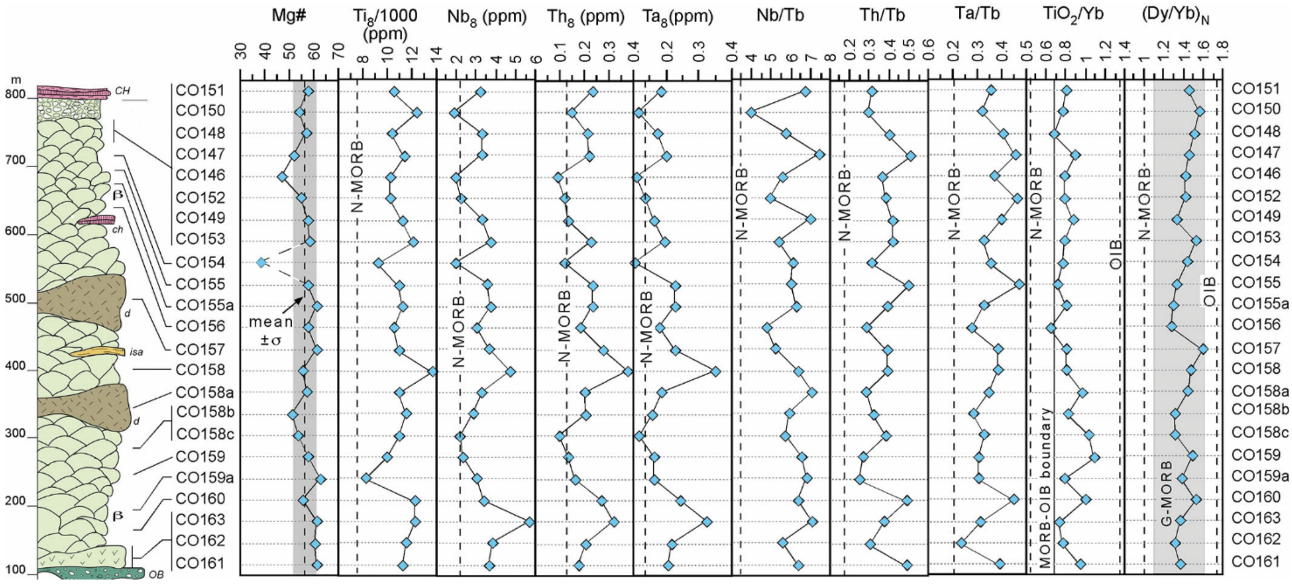

Fig. 15 - Chemostratigraphy of the Navaccia pillow lavas showing Mg# {Mg# = 100 x Mg/(Mg+Fe^{2+}), where Mg = MgO/40 and Fe = FeO/72}, selected incompatible elements, and trace element ratios. Note: sample CO154 represents the outermost section of a pillow rim; therefore, its Mg# (shaded symbol) should be used with caution because of possible mobility of Fe and Mg. Flow elevation is used a proxy for time since the flows are almost flat laying. The dashed lines represent the composition of the normal-type mid-ocean ridge basalt (N-MORB) and the ocean island basalt (OIB) of Sun and McDonough (1989); the yellow lines represent doleritic dykes cutting the pillow lava sequence; the gray field in the $(Dy/Yb)_N$ panel represents the compositional variation of garnet-influenced MORBs (G-MORB of Saccani, 2015). Dy and Yb are normalized to the chondrite composition (of Sun and McDonough (1989). Abbreviation in the stratigraphic column, CH: Red chert; b: basaltic pillow lava; d: doleritic sill; isa: silty sandstone; OB: ophiolitic breccia.

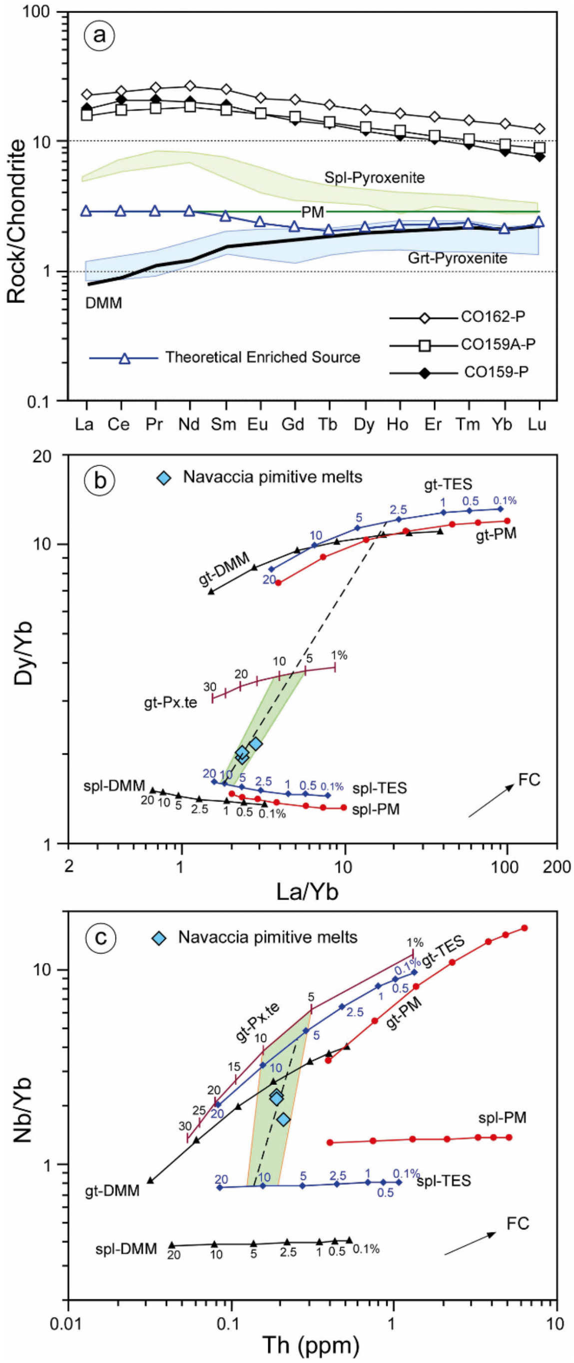

Fig. 16 - (a) Chondrite-normalized REE patterns for primary melts calculated from selected samples assuming 12 - 16% fractional crystallization of olivine + plagioclase + clinopyroxene, as well as chondrite-normalized REE patterns for the depleted MORB mantle composition (DMM; Workman and Hart (2005), the primordial mantle composition (PM; Sun and McDonough (1989), selected garnet-pyroxenites (Liu et al., 2005), and the theoretical enriched source used in the melting models shown in Figs. 16b, c. The composition of spinel-pyroxenites veins in the mantle interpreted as cumulitic rocks derived from LREE-enriched basaltic magmas (Liu et al., 2005) are shown for comparison; (b) Melting model based on La/Yb vs. Dy/Yb ratios; (c) Melting model based on Nb/Yb vs. Th. Melt curves for the garnet- (gt) and spinel (spl) facies mantle in Figs. b, c are calculated using nonmodal batch melting for various source compositions in both garnet-facies and spinel-facies mantle. Source compositions, DMM: La = 0.222 ppm, Dy =0.55 ppm, Yb = 0.353 ppm, Th = 0.009 ppm, Nb = 0.15 ppm (Workman and Hart, 2005); PM: La = 0.687 ppm, Dy = 0.737 ppm, Yb = 0.493 ppm, Th =

0.085 ppm, Nb = 0.713 ppm (Sun and McDonough, 1989), TES (theoretical enriched source): La = 0.687 ppm, Dy = 0.58 ppm, Yb = 0.353 ppm, Th = 0.018 ppm, Nb = 0.3 ppm; garnet-pyroxenite (gt-Px.te): La = 0.18 ppm, Dy = 0.30 ppm, Yb = 0.27 ppm, Th = 0.05 ppm, Nb = 0.30 ppm.
Fields indicate the arrays of the mixing between various proportions of melt fractions from garnet-pyroxenite and melt fractions from spinel-facies mantle. The dashed lines in panels c) and c) show the array of the mixing between ~2%melt fraction from garnet-facies TES and ~10%melt fraction from spinel-facies TES. Ticks on the melting curves indicate the percentages of melt fractions. Arrows indicate the fractional crystallization trends calculated assuming the crystallization of olivine, plagioclase, clinopyroxene, and spinel) in the proportions 0.08-0.45-0.45-0.02 with partition coefficients from McKenzie and O'Nions (1991). Garnet lherzolite mode is: 0.598 ol, 0.211 opx; 0.076 cpx, and 0.115 gt that melts in proportions of 0.04 ol, -0.19 opx, 1.04 cpx, and 0.11 gt. Spinel lherzolite mode is: 0.578 ol, 0.270 opx, 0.119 cpx, and 0.033 sp that melts in proportions of -0.06 ol, 0.28 opx, 0.67 cpx, and 0.11 sp. Mantle modes and melting proportions are from Kinzler (1997). Distribution coefficients for all minerals are from McKenzie and O'Nions (1991) for REE and from Ewart and Griffin (1994) for Th and Nb.

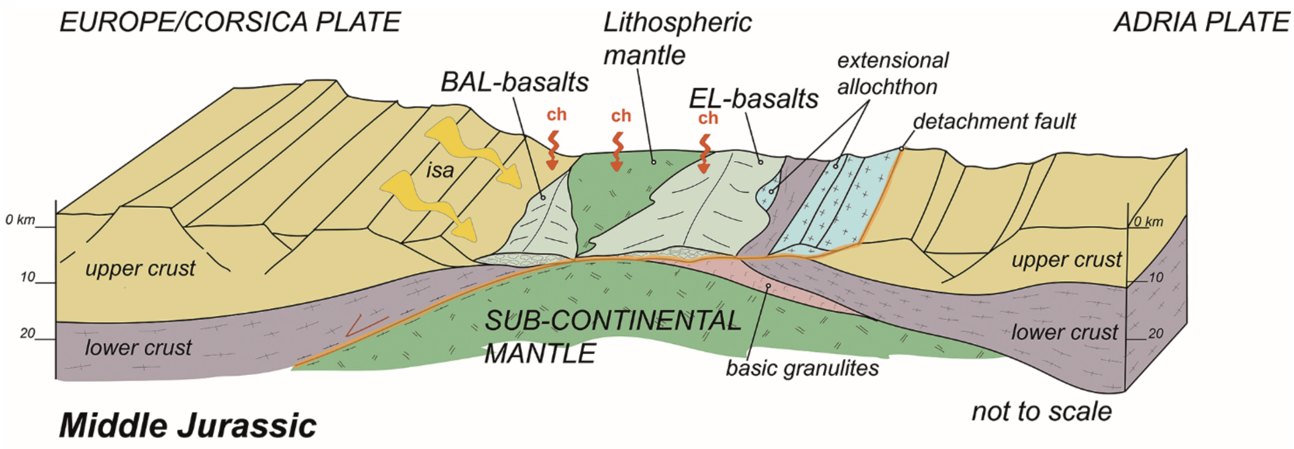

Fig. 17 - 3D snapshoot showing the location of the pillow lava basalts from both the Balagne Nappe and the External Ligurian Units formed during the initial stage of spreading in the Ligurian-Piedmont oceanic basin (Middle Jurassic). The figure shows the interference during the Middle Jurassic between volcanic activity and siliciclastic sedimentation supplied by the continental margin of Europe plate. ch: Cherts source area; isa: siltstones and silty-sandstones source area; BAL: Balagne; EL: External Ligurian. The paleogeographic location of the basalts from the Balagne nappe and the External Ligurian Units is according to Marroni and Pandolfi (2007).

Table 1 - Bulk-rock major (wt%) and trace (ppm) element analyses for basaltic rocks from the Navaccia Pillow Unit.

Sample	CO161	CO162	CO163	CO160	CO159A	CO159	CO158A	CO158B	CO158C	CO158	CO157	CO156	CO155A	CO155	CO154	CO153	CO149	CO152	CO146	CO147	CO148	CO150	CO151
Rock	bas	bas	bas	bas	bas	bas	dol	bas	bas	dol	bas	bas	bas	bas	bas	bas	bas	bas	bas	bas	bas	bas	bas
Type							dyke			dyke													
XRF analyses																							
SiO_2	49.56	49.26	50.34	50.92	49.63	48.98	51.21	49.06	51.20	50.85	49.26	50.12	50.50	49.62	48.12	51.09	51.91	51.21	49.21	51.13	54.30	54.87	51.50
TiO_2	1.85	1.90	2.00	2.04	1.36	1.64	1.82	1.91	1.83	2.26	1.79	1.74	1.86	1.79	1.59	2.02	1.86	1.72	1.68	1.89	1.76	2.05	1.76
Al_2O_3	15.98	16.07	15.62	15.83	18.27	18.14	15.47	15.02	16.75	15.63	16.34	16.40	16.37	16.04	15.50	15.76	17.08	14.81	15.68	17.85	16.79	15.60	16.48
Fe_2O_3	1.18	1.21	1.21	1.17	0.97	0.95	1.14	1.23	0.98	1.25	1.11	1.18	1.10	1.16	1.51	1.07	1.05	1.06	1.12	1.19	0.93	0.86	1.00
FeO	7.89	8.05	8.04	7.82	6.47	6.35	7.57	8.22	6.56	8.31	7.43	7.88	7.35	7.71	10.08	7.14	6.99	7.06	7.49	7.94	6.23	5.74	6.68
MnO	0.16	0.20	0.15	0.17	0.15	0.12	0.16	0.15	0.16	0.17	0.15	0.16	0.17	0.15	0.14	0.15	0.14	0.15	0.11	0.11	0.10	0.19	0.13
MgO	7.09	6.91	7.15	5.48	6.07	4.92	5.61	4.92	4.38	5.76	6.69	6.01	6.53	5.89	3.56	5.71	5.36	4.86	3.78	4.84	4.60	3.77	5.07
CaO	8.75	8.49	7.97	7.72	9.06	6.88	9.01	9.74	8.09	6.88	9.31	7.88	7.72	8.66	12.27	8.72	6.14	11.87	10.71	4.10	5.62	4.43	8.25
Na_2O	3.98	4.02	4.13	5.17	4.13	4.41	4.97	4.80	5.69	4.82	4.22	4.97	4.40	4.46	3.91	5.12	5.49	3.74	3.95	5.99	6.88	4.71	5.28
K_2O	0.47	0.76	0.63	0.32	0.65	2.05	0.12	0.43	0.57	0.75	0.20	0.07	0.93	0.28	0.92	0.10	0.56	0.07	0.09	0.65	0.15	2.55	0.56
P2O5	0.24	0.24	0.30	0.26	0.16	0.22	0.24	0.27	0.23	0.31	0.21	0.20	0.24	0.20	0.20	0.26	0.21	0.19	0.25	0.30	0.21	0.24	0.21
L.O.I.	2.73	2.82	2.39	2.96	3.03	5.28	2.75	4.32	3.46	2.91	3.26	3.32	2.91	4.00	2.07	2.69	3.11	3.22	5.90	3.97	2.12	4.88	3.05
Total	99.88	99.93	99.92	99.86	99.95	99.95	100.06	100.06	99.91	99.91	99.97	99.94	100.09	99.96	99.88	99.82	99.91	99.97	99.97	99.95	99.69	99.89	99.97
Mg#	61.6	60.4	61.3	55.5	62.6	58.0	56.9	51.6	54.3	55.3	61.6	57.6	61.3	57.6	38.6	58.8	57.7	55.1	47.3	52.1	56.8	53.9	57.5
Zn	90	99	93	97	75	86	91	100	83	95	85	88	86	88	83	89	94	79	82	89	88	97	86
Cu	52	66	44	60	56	62	56	54	62	63	57	64	57	59	41	63	72	51	59	80	71	79	67
Sc	35	32	36	38	32	33	33	36	36	39	34	36	36	39	32	39	38	33	33	37	41	42	38
Ga	18	20	19	18	15	18	19	17	21	20	15	16	19	16	17	18	15	15	16	12	12	14	14
Ni	79	86	54	53	141	45	42	59	53	35	63	65	78	67	54	61	68	64	87	127	116	78	81
Co	37	48	42	39	49	30	43	59	38	27	33	39	46	36	34	34	41	37	49	53	60	39	50
Cr	204	212	186	169	338	263	179	161	197	144	215	219	229	230	201	218	235	215	209	242	255	257	276
V	206	215	231	228	164	180	198	248	218	219	209	220	221	221	258	233	228	211	219	214	196	185	209
Ba	52	66	62	63	48	63	43	58	50	66	49	66	58	56	46	55	53	41	44	52	68	83	60
Pb	n.d	5	4	n.d	4	n.d	4	5	5	4	n.d	4	4	n.d	5	n.d	4	4	n.d	5	4	4	4
ICP-MS analyses																							
Rb	4.97	11.5	7.32	6.39	10.3	20.6	0.716	7.47	8.33	6.10	3.51	3.33	11.6	7.16	12.5	1.25	7.22	2.21	1.37	10.8	2.90	39.0	7.96
Sr	109	145	182	143	343	134	127	163	162	172	119	182	224	193	81.2	273	161	88.2	83.0	104	214	107	138
Y	23.6	31.2	34.8	28.1	21.5	22.0	25.5	28.1	22.1	36.0	29.0	33.5	28.0	30.9	26.6	32.0	25.5	25.8	28.0	26.2	34.3	36.5	27.4
Zr	115	116	134	120	81.6	110	104	133	109	146	112	124	111	109	101	147	101	111	104	115	143	133	100
Nb	4.20	4.43	6.34	5.00	4.05	3.84	4.72	4.71	3.47	6.57	4.37	4.04	4.59	4.91	4.46	5.30	4.92	3.75	4.31	5.54	5.70	4.15	5.09
La	4.82	6.10	7.44	4.69	4.36	5.07	5.82	6.12	4.23	7.34	4.00	4.86	5.56	3.97	5.27	7.35	3.78	3.95	4.96	4.57	5.17	5.14	5.74
Ce	14.0	17.0	20.2	14.4	12.2	14.9	16.0	17.3	12.9	21.8	13.6	14.0	16.0	13.0	14.4	20.1	13.0	12.4	13.9	13.5	16.1	16.1	16.6
Pr	2.30	2.79	3.31	2.62	2.00	2.38	2.66	2.89	2.15	3.82	2.38	2.38	2.59	2.26	2.42	3.42	2.25	2.18	2.31	2.32	2.76	2.91	2.74
Nd	11.5	13.9	16.6	13.1	10.0	11.2	12.4	14.1	11.1	18.7	12.0	12.9	12.8	12.2	11.8	16.7	11.5	11.3	11.5	12.1	14.4	15.1	13.4

Sm	3.49	4.28	4.97	4.07	3.03	3.39	3.69	4.24	3.49	5.43	3.86	4.09	3.84	3.75	3.75	5.02	3.47	3.58	3.53	3.80	4.61	4.80	3.97
Eu	1.12	1.41	1.56	1.29	1.07	1.09	1.06	1.39	1.06	1.53	1.19	1.29	1.22	1.09	1.13	1.51	1.10	1.13	1.13	1.28	1.54	1.53	1.27
Gd	3.96	4.75	5.51	4.58	3.63	3.47	3.84	4.65	3.58	6.00	4.78	4.99	4.29	4.65	4.25	5.96	4.18	4.37	4.47	4.56	5.95	6.24	4.64
Tb	0.657	0.790	0.894	0.779	0.592	0.586	0.670	0.793	0.597	1.03	0.834	0.849	0.733	0.812	0.729	0.974	0.706	0.755	0.768	0.745	0.987	1.04	0.758
Dy	4.08	4.97	5.62	4.76	3.68	3.54	4.14	4.77	3.62	6.28	5.37	5.29	4.62	5.07	4.51	5.94	4.36	4.72	4.80	4.72	5.94	6.48	4.81
Ho	0.818	1.02	1.12	0.942	0.758	0.716	0.831	1.00	0.753	1.29	1.05	1.13	0.959	1.07	0.942	1.19	0.919	0.963	0.986	0.963	1.19	1.34	0.957
Er	2.21	2.78	3.02	2.48	2.03	1.92	2.21	2.70	2.02	3.44	2.75	3.10	2.54	2.81	2.53	3.19	2.49	2.64	2.66	2.55	3.19	3.59	2.63
Tm	0.321	0.404	0.449	0.343	0.291	0.273	0.321	0.381	0.294	0.475	0.376	0.443	0.369	0.406	0.360	0.432	0.358	0.368	0.374	0.359	0.435	0.485	0.367
Yb	2.00	2.51	2.75	2.09	1.78	1.59	1.92	2.42	1.83	2.85	2.26	2.75	2.38	2.56	2.10	2.59	2.18	2.23	2.27	2.16	2.64	2.76	2.21
Lu	0.280	0.345	0.382	0.260	0.247	0.217	0.254	0.328	0.233	0.380	0.301	0.380	0.334	0.348	0.306	0.323	0.308	0.298	0.298	0.278	0.322	0.336	0.290
Hf	3.08	3.24	3.73	3.44	2.29	2.96	2.89	3.60	3.19	4.24	3.15	3.46	2.83	2.95	2.76	4.39	2.89	3.14	2.89	3.13	3.61	3.79	2.92
Ta	0.232	0.253	0.363	0.357	0.218	0.270	0.269	0.263	0.213	0.488	0.273	0.238	0.282	0.312	0.237	0.277	0.246	0.231	0.236	0.334	0.307	0.248	0.296
Th	0.205	0.237	0.357	0.394	0.217	0.224	0.282	0.334	0.187	0.520	0.329	0.243	0.290	0.320	0.281	0.316	0.206	0.204	0.193	0.369	0.372	0.322	0.372
U	0.076	0.083	0.135	0.114	0.082	0.098	0.097	0.124	0.083	0.193	0.083	0.074	0.098	0.110	0.150	0.107	0.089	0.076	0.099	0.144	0.141	0.077	0.134
Ti/V	56	55	53	55	52	58	57	48	52	64	53	49	52	50	38	53	51	51	49	55	55	70	52
$(La/Sm)_N$	0.89	0.92	0.97	0.74	0.93	0.97	1.02	0.93	0.78	0.87	0.67	0.77	0.93	0.68	0.91	0.95	0.70	0.71	0.91	0.78	0.72	0.69	0.93
$(Sm/Yb)_N$	1.94	1.90	2.00	2.16	1.89	2.37	2.14	1.94	2.12	2.11	1.90	1.65	1.79	1.63	1.98	2.15	1.77	1.79	1.73	1.95	1.94	1.93	1.99
$(La/Yb)_N$	1.73	1.75	1.94	1.61	1.76	2.29	2.18	1.81	1.66	1.85	1.27	1.27	1.67	1.11	1.80	2.03	1.24	1.27	1.57	1.52	1.40	1.33	1.86
Nb/Yb	2.10	1.77	2.30	2.39	2.28	2.42	2.46	1.94	1.89	2.31	1.93	1.47	1.93	1.92	2.12	2.04	2.26	1.68	1.90	2.56	2.16	1.50	2.30
Ta/Yb	0.12	0.10	0.13	0.17	0.12	0.17	0.14	0.11	0.12	0.17	0.12	0.09	0.12	0.12	0.11	0.11	0.11	0.10	0.10	0.15	0.12	0.09	0.13
Th/Yb	0.10	0.09	0.13	0.19	0.12	0.14	0.15	0.14	0.10	0.18	0.15	0.09	0.12	0.13	0.13	0.12	0.09	0.09	0.09	0.17	0.14	0.12	0.17

Abbreviations, bas: basalt; bas and: basaltic andesite; dol dyke: doleritic dyke; n.d.: not detected. Fe_2O_3 = FeO x 0.15; Mg# = 100 x Mg/(Mg+Fe2+), where Mg = MgO/40 and Fe = FeO/72. Normalizing values for REE ratios from Sun and McDonough (1989). Sample locations are shown in Fig. 3. Samples are listed in stratigraphic order from bottom (CO161) to top (CO151).

Supplementary Table S1. Comparison of major and trace element contents in reference samples analyzed using X-Ray Fluorescence spectrometry (XRF), Inductively Coupled Plasma-Mass Spectrometry (ICP-MS), as well as detection limits for all analytical methods. XRF major and tracee elements were measured on glass discs and pressed powder pellets, respectively.

		BHVO-1			JP-1			
		Recomm.	Measured Mean Values (n=33)	Relative Error (%)	Recomm.	Measured Mean Values (n=13)	Relative Error (%)	Detection limits
X-Ray Fluorescence spectrometry (XRF)	*(wt%)*							
	SiO2	49.94	49.57	0.74	42.39	42.28	0.25	0.05
	TiO2	2.71	2.74	-1.11		n.d.		0.01
	AL2O3	13.80	14.01	-1.52	0.62	0.62	-0.43	0.05
	Fe2O3	12.23	12.50	-2.21	8.34	8.34	-0.05	0.10
	MnO	0.17	0.17	0.00	0.12	0.12	0.51	0.05
	MgO	7.23	6.90	4.56	44.72	44.83	-0.25	0.01
	CaO	11.40	11.54	-1.23	0.56	0.54	2.97	0.04
	Na2O	2.26	2.34	-3.54	0.02	0.02	8.62	0.01
	K2O	0.52	0.50	3.85		n.d.		0.01
	P2O5	0.27	0.26	3.70		n.d.		0.01
	(ppm)							
	Zn	105	99	5.7	29.50	28	4.11	2
	Cu	136	140	-2.9	5.7	6	-2.92	3
	Sc	31.8	33	-3.8	7.07	7	-2.72	3
	Ga	21	22	-4.8	0.5	n.d.		3
	Ni	121	125	-3.3	2460	2526	-2.69	2
	Co	45	47	-4.4	116	111	3.92	2
	Cr	289	298	-3.1	2970	2968	0.07	2
	V	317	312	1.6	29	28	2.47	2
	Ba	139	146	-5.0	17	16	3.31	3
	Pb	2.6	n.d.		0.114	n.d.		4
Inductively Coupled Plasma-Mass Spectrometry (ICP-MS)	*(ppm)*					(n=9)		
	Rb	11.0	10.71	2.6	0.3400	0.3343	1.68	0.0020
	Sr	403	410.2	-1.8	0.5700	0.5649	0.89	0.0200
	Y	27.6	28.2	-2.3	0.1000	0.0962	3.82	0.0020
	Zr	179	190.5	-6.4	6.300	6.117	2.90	0.0300
	La	15.8	16.01	-1.3	1.200	1.136	5.35	0.0008
	Ce	39.0	37.85	2.9	0.0275	0.0275	0.10	0.0008
	Pr	5.70	5.573	2.2	0.0608	0.0591	2.71	0.0002
	Nd	25.2	26.12	-3.7	0.0077	0.0076	0.72	0.0002
	Sm	6.20	6.536	-5.4	0.0317	0.0310	2.14	0.0002
	Eu	2.06	2.111	-2.5	0.0083	0.0082	1.44	0.0002
	Gd	6.40	6.250	2.3	0.0020	0.0021	-5.75	0.0003
	Tb	0.960	0.9343	2.7	0.0101	0.0102	-1.46	0.0001
	Dy	5.20	5.395	-3.7	0.0019	0.0019	2.05	0.0001
	Ho	0.990	1.051	-6.2	0.0142	0.0142	-0.25	0.0001
	Er	2.40	2.569	-7.0	0.0035	0.0035	-0.65	0.0001
	Tm	0.330	0.3153	4.5	0.0128	0.0124	3.25	0.0001
	Yb	2.02	2.156	-6.7	0.0024	0.0024	0.56	0.0001
	Lu	0.291	0.3051	-4.8	0.0210	0.0209	0.30	0.0001
	Nb	19.0	18.48	2.7	0.0043	0.0044	-1.80	0.0003
	Hf	4.38	4.294	2.0	0.2100	0.1973	6.03	0.0003
	Ta	1.23	1.327	-7.9	0.0200	0.0204	-1.80	0.0003
	Th	1.08	1.128	-4.4	0.0120	0.0125	-4.23	0.0001
	U	0.420	0.4466	-6.3	0.0120	0.0117	2.74	0.0001

Recommended values for XRF analyses of international reference materials BHVO-1 and JP-1 are from Govindaraju (1994, Geostandard Newsletter, Special Issue, v. 118, 158 p.). Recommended values for ICP-MS analyses of the international reference material JP-1 are from Nakamura & Chang (2007, Geostandard and Geoanalytical Research, v.31, p. 185-197, doi: 10.1111/j.1751-908X.2007.00859.x). Abbreviations: Recomm. = recommended values; n.d. = not detected. Detection limits for both XRF and ICP-MS analyses were estimated using 29 international reference standards and 3 internal standards run as unknowns. In addition, detection limits for ICP-MS analyses were also checked by using procedural blanks and calculations with instrumental